AGU PUBLICATIONS

JGR

Journal of Geophysical Research: Solid Earth

RESEARCH ARTICLE

10.1002/2013JB010483

Key Points:
- The Yellowstone hotspot is fixed with respect to the North American plate motion
- North American plate velocity is between 2.30 and 2.38 cm/yr for last 10 m.y.
- New locations and timing of major eruptions on the Snake River Plain

Supporting Information:
- Table S1
- Table S2
- Figure S1

Correspondence to:
M. H. Anders,
manders@ldeo.columbia.edu

Citation:
Anders, M. H., D. W. Rodgers, S. R. Hemming, J. Saltzman, V. J. DiVenere, J. T. Hagstrum, G. F. Embree, and R. C. Walter (2014), A fixed sublithospheric source for the late Neogene track of the Yellowstone hotspot: Implications of the Heise and Picabo volcanic fields, *J. Geophys. Res. Solid Earth*, *119*, 2871–2906, doi:10.1002/2013JB010483.

Received 29 JUN 2013
Accepted 23 JAN 2014
Accepted article online 30 JAN 2014
Published online 23 APR 2014

A fixed sublithospheric source for the late Neogene track of the Yellowstone hotspot: Implications of the Heise and Picabo volcanic fields

Mark H. Anders[1], David W. Rodgers[2], Sidney R. Hemming[1], Janet Saltzman[1,3], Victor J. DiVenere[1,4], Jonathan T. Hagstrum[5], Glenn F. Embree[6], and Robert C. Walter[7]

[1]Department of Earth and Environmental Sciences and Lamont-Doherty Earth Observatory, Columbia University, Palisades, New York, USA, [2]Department of Geosciences, Idaho State University, Pocatello, Idaho, USA, [3]Science Department, Red Hook High School, Red Hook, New York, USA, [4]Department of Earth and Environmental Science, Long Island University, Brookville, New York, USA, [5]U.S. Geological Survey, Menlo Park, California, USA, [6]Department of Geology, Brigham Young University Idaho, Rexburg, Idaho, USA, [7]Department of Earth and Environment, Franklin and Marshall College, Lancaster, Pennsylvania, USA

Abstract The Heise and Picabo volcanic fields of eastern Idaho are part of the more extensive time-transgressive Yellowstone-Snake River Plain hotspot track. Calderas associated with these two silicic volcanic fields are buried under 1 to 3 km of younger basalt, so their locations and eruption record histories have been based on analysis of silicic units along the margins of the eastern Snake River Plain along with some limited geophysical data. A 1.5 km borehole penetrating through basalt into underlying silicic rocks provides new data we used to reassess caldera locations and the timing of eruptions of these volcanic fields. Using these new caldera locations, we calculate an extension-adjusted rate of 2.35 cm/yr for the North American plate over the last 6.66 m.y. and a velocity of 2.30 cm/yr over the 10.27 m.y. Recalculation of a previously determined plate velocity-based migration of the deformation field surrounding the eastern Snake River Plain yields an extension-adjusted rate of 2.38 ± 0.21 cm/yr. These migration rates all fall within the previously published range of North American plate velocities of 2.2 ± 0.8 cm/yr, 2.4 cm/yr, and 2.68 ± 0.78 cm/yr based on a global hot spot reference frame. The consistency of these rates suggest that over the last 10 m.y., the Yellowstone hot spot is fixed with respect to the motion of the North American plate and therefore consistent with a classical deep-sourced hotspot model.

1. Introduction

There is considerable debate over the cause of the track of Yellowstone-Snake River Plain volcanic system. Interpretations range from the classical model of a plume rising from deep within the mantle [*Morgan*, 1971, 1972; *Suppe et al.*, 1975; *Armstrong et al.*, 1975; *Anders et al.*, 1989; *Pierce and Morgan*, 1992, 2009; *Anders*, 1994; *Smith and Braile*, 1994; *Shervais and Hanan*, 2008; *Smith et al.*, 2009; *Obrebski et al.*, 2010, 2011] to either a shallow-sourced plume or upper mantle upwelling associated with a descending plate [*Saltzer and Humphreys*, 1997; *Humphreys et al.*, 2000; *Christiansen et al.*, 2002; *Faccenna et al.*, 2010; *James et al.*, 2011]. No matter which model for the origin of the track is proposed, it must consider the effect of the subducted Juan de Fuca plate [*Geist and Richards*, 1993]. In the classical deep-sourced model a plume head accounts for the High Lava Plain/Steens and Columbia River basalts volcanism and the tail of the plume for the Yellowstone-Snake River Plain track [e.g., *Pierce and Morgan*, 1992, 2009; *Pierce et al.*, 2002; *Camp and Ross*, 2004; *Shervais and Hanan*, 2008]. In this model the plume head disrupts the subducted plate and the plume tail breaks through providing a stable source with respect to the motion of the North American plate. However, whether the tail in these models is first represented by the McDermitt volcanic field [*Suppe et al.*, 1975; *Rodgers et al.*, 1990] or the Bruneau-Jarbidge volcanic fields [*Pierce and Morgan*, 1992; *Shervais and Hanan*, 2008] is unclear. Recent seismic tomography of the upper mantle demonstrated that the subducted plate is significantly segmented and the pattern of hot low-velocity mantle is vertically heterogeneous [*Yuan and Dueker*, 2005; *Yuan et al.*, 2010; *Wagner et al.*, 2010; *Obrebski et al.*, 2010; *James et al.*, 2011; *Obrebski et al.*, 2011; *Schmandt et al.*, 2012]. These studies of mantle structure suggest that below ~200 km, there is a low-velocity or hot mantle conduit that is deflected from directly below the track of the Yellowstone-Snake River Plain track, but by the 660 km discontinuity is either directly under Yellowstone or at least closer to the Yellowstone-Snake River Plain track than in the overlying transition zone higher-velocity mantle. One recent study suggested that a tear in the

subducted plate creates a gap through which hot mantle rises off the descending plate edge resulting in the Yellowstone-Snake River Plain volcanic system [*James et al*., 2011]. However, *Schmandt et al*. [2012] demonstrated a rise of the 660 km discontinuity under Yellowstone consistent with a rising plume and *Obrebski et al*. [2011] imaged a low-velocity zone extending down to at least 900 km under Yellowstone.

A fixed deep-sourced hotspot model is in part based on early studies of oceanic volcanic tracks that exhibit a regularly spaced progression tied to movement of lithospheric plates [e.g., *Morgan*, 1971]. Later discoveries of high $^{3}He/^{4}He$ ratios further supported the notion that hotspots were sourced deep in the mantle [e.g., *Class and Goldstein*, 2005]. Although the $^{3}He/^{4}He$ ratios are consistent with a deep source of a Yellowstone plume [see *Graham et al*., 2009; cf. *Christiansen et al*., 2002], there is a problem with the progression of silicic volcanism as it tracks across the North American plate. If initiation of the silicic Yellowstone-Snake River Plain volcanic track is at the McDermitt volcanic field located in northwestern Nevada/southeast Oregon as suggested by *Suppe et al*. [1975], *Rodgers et al*. [1990], and *Pierce and Morgan* [1992], then the rate of track progression is significantly greater than predicted by independent estimates of North American plate velocity [*Minster and Jordan*, 1978; *Gripp and Gordon*, 1990, 2002]. However, at some point the rate of volcanic progression should stabilize to a rate consistent with North American plate velocity if the Yellowstone hotspot is fed by a plume that is deep sourced and fixed. The track rates for the Yellowstone-Snake River Plain silicic volcanic system are for the most part based on the location of poorly defined volcanic centers [e.g., *Pierce and Morgan*, 1992]. However, using the progress of the thermally activated deformation field surrounding the eastern Snake River Plain yields much lower rates, closer to those track-independent rates [*Minster and Jordan*, 1978; *Gripp and Gordon*, 1990, 2002; *Anders*, 1994; *Rodgers et al*., 2002].

To address the discrepancy between velocities derived from global fixed reference frame models, the deformation field velocity, and the velocity determined using silicic caldera locations we have relocated two key caldera in the Picabo and Heise volcanic fields from which previous rate estimations have been made. The new locations result in silicic volcanism migration rates for the last 10 m.y. of silicic volcanism nearly equivalent to rates determined using methods not involving caldera locations. We also recalculated the progression of the deformation field using these new age constraints. These data taken together show that the Yellowstone-Snake River Plain volcanic system behaves in a manner consistent with a stable hotspot plume being overridden by the North American plate for the majority of its history.

2. Geologic Setting

2.1. Heise and Picabo Volcanic Fields

The Heise and Picabo volcanic fields are composed of a series of silicic ashfall tuffs, ignimbrites, and rhyolite lavas interbedded with terrestrial and volcaniclastic sediments that are exposed on the margins of the eastern Snake River Plain of east-central Idaho (Figures 1 and 2a). *Kirkham* [1927, 1931] first described these units as the rhyolitic "Tertiary Late Lavas" which he suggested were continuous from outcrops north of the eastern Snake River Plain to outcrops to the south and buried under more than half a kilometer of Pliocene-Quaternary basalt near the center of the eastern Snake River Plain. The ignimbrites discussed in this paper range from 10.41 ± 0.01 Ma to 7.58 ± 0.01 Ma for the Picabo volcanic field and from 6.66 ± 0.01 Ma to 4.61 ± 0.01 Ma for the Heise volcanic field. Along the margins of the eastern Snake River Plain there are several basalt and andesite deposits that due to their spatial and temporal positioning we consider to be associated with Picabo and Heise volcanic field volcanism. Examples of these andesites include the 6.0 Ma hypabyssal Calamity Point Andesite in Swan Valley, Idaho, [*Armstrong et al*., 1975; *Anders et al*., 1989, Figure 2] and several andesites found in the Jackson Hole area [*Love et al*., 1992]. Also associated with these two volcanic fields are several basalt flows found off the eastern Snake River Plain such as the 9.9 Ma Howe Point Basalt, the 7.51 Ma Briggs Canyon Basalt, the 7.03 Ma Lone Pine Basalt, and the 5.4 Ma Scott Butte Basalt (Figure 2a) (a more detailed location of these basalts are in *Rodgers and Anders* [1990] and *Anders et al*. [1993]).

The Picabo and Heise volcanic fields have been extensively studied since 1927 by workers including *Kirkham* [1927, 1931], *Mansfield and Ross* [1935], *Armstrong et al*. [1975], *Prostka and Embree* [1978], *Prostka et al*. [1979], *Doherty et al*. [1979], *McBroome* [1981], *Embree et al*. [1982], *Williams et al*. [1982], *Leeman* [1982a, 1982b], *McBroome et al*. [1982], *Morgan et al*. [1984], *Kellogg and Embree* [1986], *Hackett and Morgan* [1988], *Morgan* [1988], *Anders et al*. [1989], *Rodgers and Anders* [1990], *Pierce and Morgan* [1992], *Morgan* [1992], *Anders and Sleep* [1992], *Anders et al*. [1993], *Kellogg et al*. [1994], *Pierce et al*. [2002], *Rodgers et al*. [2002],

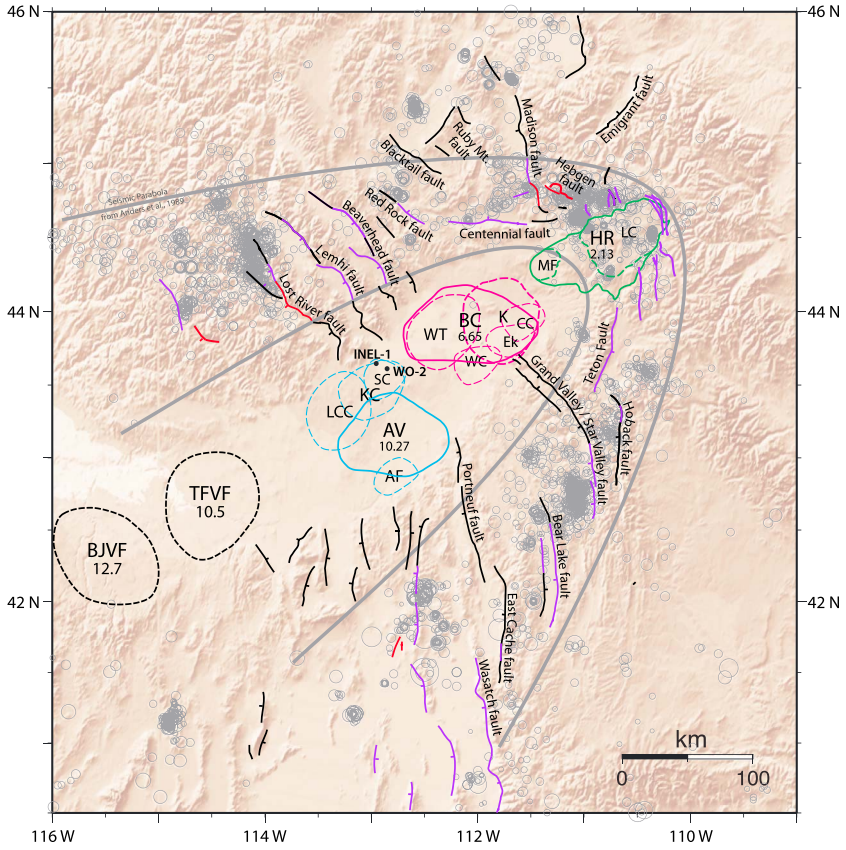

Figure 1. Estimated location of calderas associated with silicic eruptions of the track of the Yellowstone hotspot. Yellowstone volcanic field calderas are in green, Heise volcanic field calderas are in red, and the Picabo volcanic fields are in blue. Size and location of the calderas are based on regional extent of eruptive products and their proximal or distal characteristics. Faults that ruptured during historic earthquakes are in red, purple for faults that offset latest Quaternary deposits, and black is for faults with Neogene to the latest Quaternary offset. Fault and earthquake locations are from *Simpson and Anders* [1992], seismic parabolas are from *Anders et al*. [1989], and caldera locations are modified from *Anders et al*. [2009]. Letters on calderas correspond to the following: LC (649 ka Lava Creek), MF (1.30 Ma Mesa Falls), HR (2.13 Ma Huckleberry Ridge Tuff), K (4.61 Ma Kilgore Tuff), ES (5.52 Ma tuff of Elkhorn Spring), WC (5.72 Ma tuff of Wolverine Creek), CC (6.01 Ma Conant Creek Tuff), WT (6.27 Ma Walcott Tuff), BC (6.66 Ma Blacktail Creek Tuff), AF (7.58 Ma tuff of American Falls), LRS (8.87 Ma tuff of the Lost River Sinks), KC (9.28 Ma tuff of Kyle Canyon), LCC (9.46 Ma tuff of Little Chokecherry Canyon), AV (10.27 Ma Arbon Valley Tuff), TFVF (Twin Falls volcanic field 12.5 Ma to 7.5 Ma), and BJVF (~12.5 Ma Bruneau-Jarbidge volcanic field). Locations of the Twin Falls and Bruneau-Jarbidge volcanic fields are from *Bonnichsen et al*. [2008], and the Yellowstone volcanic field from *Christiansen* [2001].

Morgan and McIntosh [2005], *Bindeman et al*. [2007], *Branney et al*. [2008], *Bonnichsen et al*. [2008], *Pierce and Morgan* [2009], *Watts et al*. [2010], *Watts et al*. [2011], and *Drew et al*. [2013]. Of these studies *Morgan and McIntosh* [2005] provide the most extensive study of the Heise volcanic field and thus provide the closest comparison to our study of these units. However, several of the unit names of the Heise volcanic field used here are different than used by other authors, including *Morgan and McIntosh* [2005], and these differences are discussed below and in *Anders et al*. [2009]. The Picabo volcanic field is less well studied although *Drew et al*. [2013] provided a compilation of the Picabo volcanic field volcanic units with an emphasis on their geochemistry while also providing some important U/Pb age dating of these units.

One of the largest units of the Heise volcanic field eruptions is the 6.66 Ma Blacktail Creek Tuff. It has the greatest distance between welded tuff outcrops, and we estimate an estimated maximum volume of ~1500 km^3 [cf. *Morgan and McIntosh*, 2005] placing it on par with the Huckleberry Ridge Tuff B eruption, the most voluminous of the three 2.13 Ma Huckleberry Ridge Tuff eruptions of the Yellowstone volcanic field [*Christiansen*, 2001; *Ellis et al*., 2012] age converted to a common reference age of 2.127 ± 0.006 Ma using the Fish Canyon Tuff standard and decay constants from *Kuiper et al*. [2008]. The largest unit of the Picabo

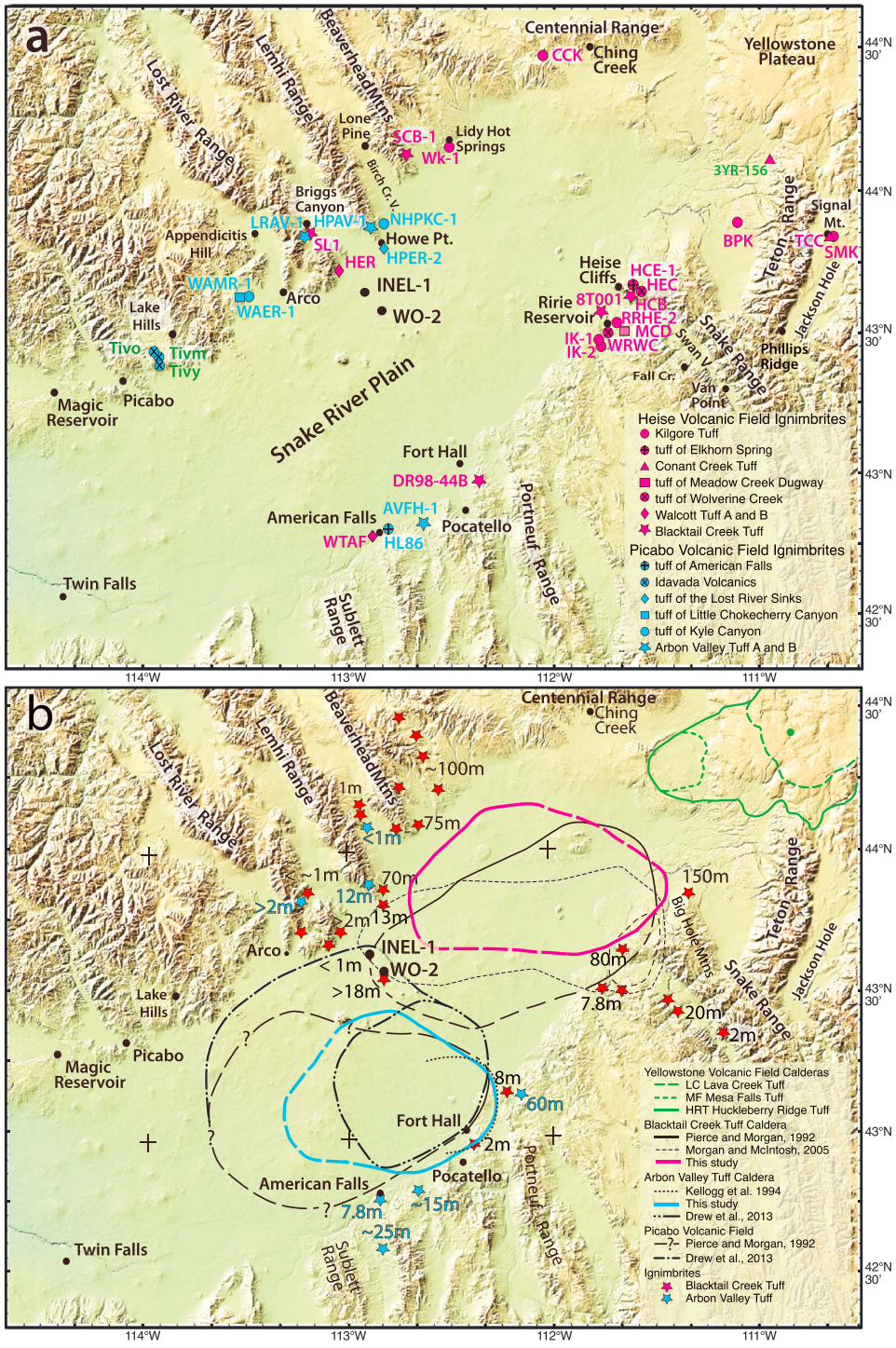

Figure 2. Volcanic rocks of the eastern Snake River Plain. (a) Location of sites sampled for $^{40}Ar/^{39}Ar$ analysis. Sites with red symbols are from the Heise volcanic field, blue symbols are for the Picabo volcanic field, and green represents sampling sites from other studies discussed in the text. Black lettering and solid black circles represent features discussed in text. (b) Caldera boundaries for the Blacktail Creek Tuff are from *Pierce and Morgan* [1992], black partially dashed, *Morgan and McIntosh* [2005], black short dashes, and this paper, in red. For the Arbon Valley Tuff caldera location, dotted black line is from *Kellogg et al.* [1994], black dashed lines with quarries is the Picabo volcanic field from *Pierce and Morgan* [1992], dashed with a single dot between lines is the Picabo volcanic field from *Drew et al.* [2013], the dashed lines with three dots is the Arbon Valley Tuff Caldera (Tabor Caldera) from *Drew et al.* [2013], and blue lines are from this study. Thickness of units at sampling sites (in meters) are from *Stearns and Isotoff* [1956], *Carr and Trimble* [1963], *Prostka and Embree* [1978], *Skipp* [1984], *Piety et al.* [1986], *Hladky et al.* [1992], *Hough* [2001], *Morgan and McIntosh* [2005], *Price* [2009], and the authors' field measurements.

volcanic field produced the Arbon Valley Tuff which, as we will discuss below, may record two eruptive events. Due to limited exposure, any estimate of its volume is speculative until more data is available.

Outcrops from the Picabo and Heise volcanic fields are irregularly distributed along both margins of the eastern Snake River Plain. However, because a young basalt field 80 km wide and 1 to 3 km thick separates the margins and overlies the calderas associated with these volcanic fields correlating units is difficult. To aid correlation, we analyzed rhyolite from north to south margins as well as core from the WO-2 drill hole located near the center of the eastern Snake River Plain. The WO-2 core contains a nearly complete record of ignimbrite eruptions of the Heise volcanic field, thus facilitating correlation. Here we use $^{40}Ar/^{39}Ar$ geochronology, paleomagnetic analysis, feldspar geochemistry, and thin section petrology to correlate between outcrops and the WO-2 core. The established correlations are then used to estimate the regional extent of these eruptions, locate individual calderas, and determine a new estimate of the migration rate of Yellowstone-Snake River Plain volcanism during the last 10 m.y.

2.2. Previous Estimates of Rates

Armstrong et al. [1975] were the first to estimate a migration velocity of the Yellowstone-Snake River Plain volcanism at 3.5 cm/yr. *Suppe et al.* [1975] used the *Armstrong et al.* [1975] data to recalculate a rate of 2.5 cm/yr. Using newer ages from various studies, *Rodgers et al.* [1990] calculated an average migration velocity of 4.5 cm/yr over 16 m.y. using caldera locations and 3.7 cm/yr after accounting for hotspot track-initiated extension along the margins of the eastern Snake River Plain, significantly higher than independent rate estimates of North American plate motion of *Minster and Jordan* [1978] and *Gripp and Gordon* [1990, 2002] of 2.4 cm/yr, 2.2 cm/yr, and 2.68 cm/yr, respectively. *Pierce and Morgan* [1992] compiled a few more volcanic ages and were the first to suggest two migration rates, a fast rate of 7 cm/yr prior to 10 Ma and a 2.9 cm/yr migration rate based on a linear fit to the Yellowstone, Heise, and Picabo volcanic fields during the last 10 m.y. They assumed the hotspot track initiated at the McDermitt Volcanic Center along the Nevada/Oregon thereby resulting in the higher initial rates. *Geist and Richards* [1993], *Camp and Ross* [2004], *Pierce et al.* [2002], and *Pierce and Morgan* [2009] have suggested the higher initial rates were due to interference of the hotspot head with the downgoing Juan de Fuca plate.

Allmendinger [1982] first documented northeastward migration of the deformation field adjacent to the volcanic track, based on the age of Basin and Range extension in four locations; *Rodgers et al.* [1990] expanded this analysis to document a pulse of extension that occurred ahead of, and beside, the migrating hotspot. *Anders* [1994] presented an integrated model of extension and volcanism that interprets the tectonic or seismic parabola (Figure 1) as a migrating region of accelerated faulting due to the thermal effects of the hotspot and derived a 2.2 ± 0.18 cm/yr rate for the last 10 m.y. interval. *Rodgers et al.* [2002] calculated an extension rate of 0.4 to 0.6 cm/yr in the region surrounding the eastern Snake River Plain, which they subtracted from the estimate of *Pierce and Morgan* [1992] of 2.9 cm/yr resulting in a plate migration rate since 10 Ma of 2.3 to 2.5 cm/yr.

Using hotspot reference frames, *Minster and Jordan* [1978] and *Gripp and Gordon* [1990] determined a North American plate migration rate of 2.4 cm/yr and 2.2 ± 0.18 cm/yr, respectively, for intervals younger than 10 m.y. *Gripp and Gordon* [1990] used the volcanic-center-independent data in their HS2 NUVEL1 worldwide velocity model over the last 3 m.y. *Gripp and Gordon* [2002] determined a higher volcanic-center-independent rate for the last 5.8 m.y. of 2.68 ± 0.78 cm/yr using their newer HS3-NUVEL1A compilation. While the former rates are comparable to migration rates of the deformation field [*Anders*, 1994; *Rodgers et al.*, 2002], they are significantly slower than migration rates of volcanism calculated by using the previous position and timing of buried calderas of the Yellowstone-Snake River Plain silicic volcanic system. As we will suggest below, our new interpretation of the locations of these buried calderas places them more to the northeast and thus more in line with lower estimates of North American plate velocity and more in line with a fixed-source hotspot model for the last 10 m.y.

2.3. WO-2 Core

In 1990 a 1.5 km borehole (WO-2) was drilled into the eastern Snake River Plain (Figures 1 and 2) on the Idaho National Laboratory property [*Mazurek*, 2004] called INEL at the time of drilling. Core from WO-2 had near 100% recovery from the surface to 1524 m (5000 ft). The upper 1143 m (3750 ft) encountered basalts and sedimentary interbeds. Below 1143 m (3750 ft) the core encountered only silicic volcanic rock with rare sediment interbeds. As we will discuss below, in WO-2 we have identified six Heise volcanic field ignimbrite units, five of which are found along the margins of the eastern Snake River Plain including the 6.66 Ma

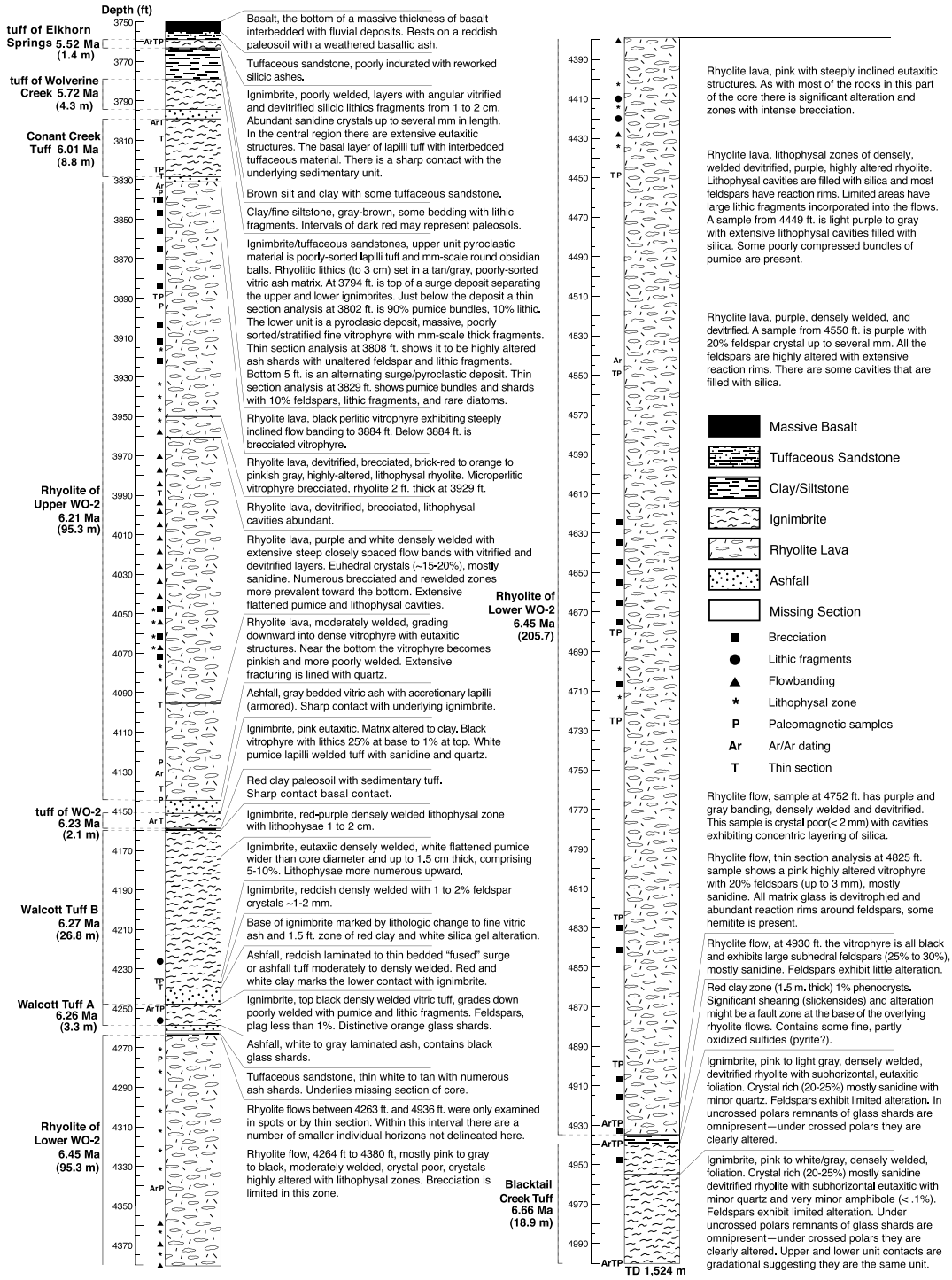

Figure 3. Stratigraphy of the WO-2 drill core. Core is labeled in feet (as this was how the core was measured during recovery), and thicknesses of individual units are in meters. There are likely more individual rhyolite lavas than shown, as limited effort was placed on separating one lava from another. Descriptions were based on analyses by Glenn Embree and Mark Anders and in part from data from *Anders et al.* [1997] for which core descriptions were provided by coauthor William C. Hackett.

Blacktail Creek Tuff, the oldest of the Heise volcanic field ignimbrites, at the bottom of the core (Figure 3). We also observed one previously unidentified ignimbrite and two thick rhyolite lavas. We studied the core using $^{40}Ar/^{39}Ar$ age dating, paleomagnetism, feldspar geochemistry, and thin section analysis. We use these data to correlate core rocks to various units found on the margins of the eastern Snake River Plain. In doing so, we

identify some discrepancies in correlations north and south of the eastern Snake River Plain, and by analyzing the petrography of the recovered core, we were able to more precisely constrain caldera locations of the Heise volcanic field, some of which we suggest are closer to the Yellowstone Plateau than previously thought.

2.4. Volcanic Field Nomenclature

The ignimbrites of the Heise volcanic field have been assigned an unusually large number of different names since they were first identified by *Kirkham* [1927, 1931], e.g., the Blacktail Creek Tuff has had at least seven different names. Some name changes acknowledge that units north of the Snake River Plain should be correlated to those south of the Plain. Some name changes are due to subdivision of previously named units, and some seemed to have changed for no logical reason. Ignimbrites, like many geologic units, have common usage names that are not based on priority structure. Here we used the "formalized" names for several units for which we had previously used a priority-based nomenclature. These units include the Blacktail Creek Tuff and the Kilgore Tuff [e.g., *Morgan and McIntosh*, 2005]. In previous studies we have called these units the tuff of Edie School and tuff of Heise, respectively, based on our understanding of their priority structure [*Anders et al*., 1997, 2009]. Here we also have identified ignimbrites that have isotopic ages, paleomagnetic orientations, and chemistries that are sufficiently distinct to subdivide them into discrete eruptive events (e.g., Walcott Tuff A and Walcott B, and Arbon Valley Tuff A and Arbon Valley B). We will discuss this in more detail later in the text.

3. Methods

3.1. Argon-40/Argon-39 Chronology

In addition to age dating of rocks from various depths in the WO-2 core, we dated a number of silicic ignimbrites and ashfall deposits, basalts, and andesites along the margins of the eSRP. The $^{40}Ar/^{39}Ar$ analyses were done at the Berkeley Geochronology Center (then at the Institute of Human Origins) in Berkeley, California, and at the Argon Geochronology for the Earth Sciences (AGES) Laboratory at Lamont-Doherty Earth Observatory of Columbia University by laser fusion of single grains. After fusion in an ultrahigh vacuum, aliquots of gas liberated from the mineral melts were exposed to Zr-Fe-V and Zr-Al sintered metal alloy getters to remove reactive gases. The remaining inert gasses, principally argon, were then admitted to the mass spectrometer, and the argon-isotopic ratios were determined by peak hopping on a single analog multiplier using automated data collection software (MassSpec) developed by Al Deino of the Berkeley Geochronology Center. Samples were corrected for background and mass discrimination based on repeated measurements of full system blanks and air pipettes, respectively. Samples are corrected for nuclear interferences using the published data from the reactor [*Renne et al*., 1998]. Many samples were partially digested in short-duration dilute HF baths, and several samples were analyzed by step heating for comparison to single-step ablation data. One of the key differences between various laboratories is the use of different standards. Here we used sanidine from Fish Canyon Tuff of central Colorado as a standard to establish our calibration (*J* value) with an interlaboratory accepted age of 28.201 ± 0.046 Ma for the Fish Canyon Tuff [see *Kuiper et al*., 2008]. Other laboratories use slightly different ages for the same standard. For example, *Morgan and McIntosh* [2005] used an age of 27.84 Ma for the Fish Canyon Tuff. A similar standard was used at the Berkeley Geochronology Center for some of our samples from WO-2. All our age determinations were calculated or recalculated using the newer 28.201 ± 0.046 Ma standard age [see *Kuiper et al*., 2008] with the recommended decay constants from *Min et al*. [2000]. We also converted $^{40}Ar/^{39}Ar$ ages from other studies to a common 28.201 ± 0.046 Ma standard for the Fish Canyon Tuff including the data from *Morgan and McIntosh* [2005] and *Ellis et al*. [2012] for the Huckleberry Ridge Tuff A using $\lambda = 5.463E\text{-}10 \pm 1.07E\text{-}11$ and Noah McClean ArArReCalc 7/31/09. Our error estimates are 1 σ whereas Morgan and McIntosh's are 2 σ. We are aware that the accepted age of the Fish Canyon sanidine standard, as well as the K-40 decay constants, have been in flux [e.g., *Renne et al*., 2010, 2011; *Channell et al*., 2010], but since all dates reported here were calculated with the same standard ages and constants, we are confident in our ability to precisely detect differences in measured ages among unknown sample populations. In most cases where the age determined was either significantly too old or too young from the bulk of the samples analyzed, we did not report them here except for samples from the WO-2 core, in order to get a sense of the consistency of the results from our limited WO-2 sampling. Errors in the case of multiple samples were calculated using *Taylor* [1982] statistics.

3.2. Paleomagnetic Analysis

All paleomagnetic field sampling was done using a Pomeroy gas-powered drill with a minimum of seven individual cores at each site recovered from different locations along the same outcrop. Wherever possible, samples were taken from a basal vitrophyre where secondary magnetization and compaction have the least effect on the remnant direction [e.g., *Rosenbaum*, 1986]. Sampling from the WO-2 core (Figure 3), on the other hand, was done in the laboratory where samples were drilled at right angles to the vertical core sections using a drill press. Paleomagnetic analyses were carried out at the U.S. Geological Survey (USGS) laboratory in Menlo Park for all sampling sites other than for the WO-2 core. Samples from the WO-2 core were analyzed at the Lamont-Doherty Paleomagnetics Laboratory of Columbia University. Natural remnant magnetizations (NRMs) were measured from all samples, and all samples were subsequently subjected to alternating field (Af) demagnetization typically to peak inductions between 50 mT and 90 mT. *Anders et al*. [1993] have established unit mean directions for the Kilgore Tuff, the Walcott Tuff B, and the Blacktail Creek Tuff, the three largest of the Heise volcanic field eruptions. The unit means were calculated by using sampling sites where underlying and overlying bedded units could be found in order to establish paleohorizontal. Several other studies have reported only site mean directions for these units [e.g., *McBroome*, 1981; *Morgan*, 1988, 1992; *Morgan and McIntosh*, 2005]. Mean directions for sites in the eastern Snake River Plain cannot be averaged to determine a correct unit mean from randomly selected sites because there is a strong northeast tectonic tilt to almost all samples as demonstrated by *Anders et al*. [1989, 1993], *Rodgers and Anders* [1990], *Rodgers et al*. [1990, 2002] and *Anders* [1994].

The WO-2 drill core was not oriented with respect to declination during recovery, thus, the paleomagnetic declinations determined for each depth drilled cannot be used compared to mean site directions determined by *Anders et al*. [1993]. However, each contiguous section of core analyzed included at least three paleomagnetism samples, and thus K, R, and α_{95} values using *Fisher* [1953] were calculated. A statistical approach of *Arason and Levi* [2010] for calculating solutions for inclination-only data was used to characterize inclination for each unit within the WO-2 core. Moreover, since WO-2 was drilled within a degree of vertical [*Mazurek*, 2004], the inclination and polarity for each sampled core section provides useful information for purposes of ascertaining tectonic tilt information.

3.3. Feldspar Geochemical Analysis

We analyzed feldspars for major elements using an electron microprobe at Lamont-Doherty Earth Observatory. Feldspars samples came from four ignimbrites and one rhyolite lava from the margins of the eastern Snake River Plain, and four ignimbrites and two rhyolite lavas in WO-2. Several of the samples from WO-2 were of the same unit as sampling was done prior to establishing unit identities. We also compared our results to those from a microprobe analysis of five ignimbrites from *Henshaw* [2002]. The choice of feldspar as a representative mineral was in part dictated by its abundance in all the ignimbrites and rhyolite lavas studied. Samples were mounted as thin sections, and visible feldspar grains were analyzed in each sample. Between five and 12 grains were analyzed from each sample, and four to six points were analyzed from core to rim of each grain. The majority of analyses were on units within the WO-2 core with a few analyses on major ignimbrites of the Heise and Picabo volcanic fields. We only analyzed the youngest of the ignimbrites of Picabo volcanic field, the 7.58 Ma tuff of American Falls. *Henshaw* [2002] analyzed Arbon Valley Tuff thus providing two samples from the Picabo volcanic field.

Primary minerals have been shown to be in similar proportions throughout the ignimbrites and lavas thus permitting characterization of these units based on crystal populations and composition [e.g., *Hildreth*, 1977]. We have used this to our advantage in correlating the ignimbrite units found in the WO-2 borehole (Figure 3) to units found in the region surrounding the Snake River Plain. Whole-rock rare earth element (REE) analysis was previously performed on some of the larger eruptions of the Heise volcanic field such as the 4.61 Ma Kilgore Tuff, the 6.27 Ma Walcott Tuff, and the 6.66 Blacktail Creek Tuff [*Morgan et al*., 1984; *Anders et al*., 1989] which showed a general increase in REEs from the oldest to the two youngest units. Studies using whole-rock X-ray fluorescence techniques determined concentrations of zirconium and several other trace elements [*Morgan*, 1992]. Studies of $\delta^{18}O$ were done on some of the ignimbrites in an attempt to correlate. For example, *Morgan* [1992] used $\delta^{18}O$ to correlate various ignimbrites of the Heise volcanic field such as her correlation of the tuff of Elkhorn Spring and the Conant Creek Tuff. *Bindeman et al*. [2007] suggest that progressive lowering of $\delta^{18}O$ within cycles represents reincorporation in

Table 1. Heise Volcanic Field Ignimbrites $^{39}Ar/^{40}Ar$ Isotopic Ages

Sample	40/39	37/39	36/39	40*/39	%Rad	Age	Error	Irrad.	*J*	Ar40	Ar40 Moles
IK-1 (Ione)											
20053-01	1.97415	1.3263	0.0007	1.8485	93.5	4.48	0.04	6	0.0013800	0.2281	2.10E-15
20053-02	2.25261	1.3792	0.0016	1.8766	83.2	4.52	0.05	6	0.0013800	0.1249	1.15E-15
20053-03	1.97330	0.9094	0.0005	1.8949	96.0	4.57	0.04	6	0.0013800	0.1790	1.65E-15
20053-04	3.61067	1.6046	0.0064	1.8222	50.4	4.66	0.14	6	0.0013800	0.0363	4.50E-16
20053-05	3.33986	1.2376	0.0047	2.0117	60.2	4.59	0.12	6	0.0013800	0.1151	1.06E-15
20053-06	3.4946	0.4074	0.0051	1.9987	57.2	4.84	0.10	6	0.0013800	0.1121	1.03E-15
						Ave. 4.55 ± 0.02 Ma					
IK-2 (Ione)											
20059-01	3.89799	1.3034	0.0069	1.9316	49.5	4.66	0.18	6	0.0013800	0.0782	7.20E-16
20059-02	3.32274	0.6172	0.0049	1.9038	57.3	4.59	0.05	6	0.0013800	0.2207	2.03E-15
20059-03	3.46838	0.1040	0.0051	1.9647	56.6	4.40	0.08	6	0.0013800	0.2590	3.25E-15
20059-04	8.77340	0.8809	0.0235	1.8789	21.4	4.57	0.38	6	0.0013800	0.1100	1.01E-15
20059-05	2.52248	1.2280	0.0019	2.0233	80.1	4.83	0.21	6	0.0013800	0.0229	2.10E-16
20059-06	2.08484	0.3534	0.0007	1.8910	90.7	4.56	0.06	6	0.0013800	0.0643	5.90E-16
20059-07	4.24239	0.0680	0.0075	2.0315	47.9	4.61	0.08	6	0.0013800	0.2829	3.55E-15
						Ave. 4.56 ± 0.03 Ma					
RRHE-2 (Riere Reservoir, Meadow Creek Dugway)											
12229-02	1.16092	0.0416	0.0004	1.0350	89.2	4.76	0.06		0.0026210	0.0471	6.59E-15
12229-03	1.27766	0.3570	0.0011	0.9672	75.7	4.72	0.07		0.0026210	0.0424	5.96E-15
						Ave. 4.74 ± 0.05 Ma					
CCK (Camas Creek)											
20145-01	8.81883	3.4853	0.0189	2.8557	34.7	4.56	1.61	m2	0.0008743	0.0078	7.00E-17
20145-03	6.94242	2.6125	0.0144	2.8658	41.2	4.57	0.48	m2	0.0008743	0.0210	1.30E-16
						Ave. 4.57 ± 0.46 Ma					
SMK (Signal Mountain)											
15570-11A	1.47520	0.08378	0.0025	0.1600	98.3	4.44	0.37	29D	0.0017001	0.0235	1.60E-15
15570-12A	1.53825	0.08878	0.0032	0.3040	98.7	4.65	0.19	29D	0.0017001	0.0466	3.04E-15
15570-13A	1.56444	0.08813	0.0042	0.3330	94.7	4.53	0.18	29D	0.0017001	0.0521	3.33E-15
15570-14A	1.49584	0.07981	0.0007	0.2110	102.7	4.70	0.28	29D	0.0017001	0.0315	2.11E-15
15570-15A	1.47998	0.30285	0.0030	0.0990	103.5	4.69	0.59	29D	0.0017001	0.0146	9.89E-16
15570-18A	1.66781	0.08297	0.0057	0.0730	89.4	4.56	0.81	29D	0.0017001	0.0121	7.62E-16
15570-19A	1.48119	0.08707	0.0015	0.0650	103.3	4.68	0.90	29D	0.0017001	0.0097	6.55E-16
15570-22A	1.58141	0.41583	0.0026	0.1680	96.4	4.67	0.34	29D	0.0017001	0.0265	1.68E-15
15571-03A	9.34118	2.14237	0.0158	0.0290	94.4	4.58	0.09	29D	0.0017001	0.0188	1.99E-16
15571-04A	1.88092	0.53128	0.0043	0.2640	91.1	4.61	0.91	29D	0.0017001	0.0236	1.24E-15
						Ave. 4.58 ± 0.07 Ma					
Wk-1 (Lidy Hot Springs)											
20162-01	3.17130	0.0888	0.0016	2.6886	84.8	4.38	0.07	m2	0.0008743	0.1126	9.50E-16
20162-02	3.71869	0.0463	0.0029	2.8422	76.4	4.55	0.02	m2	0.0008743	0.1102	1.37E-15
20162-03	2.92233	0.0405	0.0004	2.8121	96.2	4.57	0.09	m2	0.0008743	0.0822	1.00E-15
12227-01	1.53357	0.8402	0.0023	0.9017	58.8	4.43	0.23		0.0026210	0.0148	2.05E-15
12227-02	1.11780	0.0443	0.0006	0.9442	84.5	4.55	0.06		0.0026210	0.0459	6.41E-15
12227-03	1.21483	0.0494	0.0009	0.9533	82.4	4.76	0.17		0.0026210	0.0190	2.65E-15
12227-04	1.16500	0.0472	0.0004	1.0376	89.1	4.92	0.23				
						Ave. 4.54 ± 0.02 Ma					
BPK (West flank of the Teton Range)											
15569-03A	1.52333	0.0298	0.02983	3.4160	99.0	4.62	0.02	29D	0.0017001	0.5205	3.42E-14
15569-04A	1.52884	0.03054	0.00254	4.2300	98.8	4.62	0.02	29D	0.0017001	0.6460	4.23E-14
15569-05A	1.53093	0.02883	0.00291	2.2960	99.1	4.64	0.03	29D	0.0017001	0.3513	2.30E-14
15569-06A	1.74006	2.06805	0.00302	0.2340	82.7	4.40	0.26	29D	0.0017001	0.0406	2.34E-15
15569-07A	1.56121	0.02841	0.00291	2.7030	99.8	4.77	0.02	29D	0.0017001	0.4216	2.70E-14
15569-08A	1.58601	0.03171	0.00344	1.3920	97.0	4.71	0.05	29D	0.0017001	0.2206	1.39E-14
15569-09A	1.56433	0.02649	0.00338	1.1570	98.4	4.71	0.05	29D	0.0017001	0.1809	1.16E-14
15569-10A	1.52488	0.02791	0.00327	0.8690	99.2	4.63	0.07	29D	0.0017001	0.1324	8.69E-15
15569-11A	1.53505	0.03495	0.00269	1.4010	99.1	4.65	0.04	29D	0.0017001	0.2149	1.40E-14
Kilgore Tuff						*Ave. 4.66 ± 0.01 Ma*					
						Ave. 4.61 ± 0.01 Ma					
HCE-1 (Heise Cliffs)											
20142-02	4.73688	0.0246	0.0045	3.3791	71.3	5.45	0.02	m2	0.0008743	0.2082	1.76E-15
20142-03	3.96097	0.0207	0.0024	3.2325	81.6	5.23	0.17	m2	0.0008743	0.0323	2.70E-16

Table 1. (continued)

Sample	40/39	37/39	36/39	40*/39	%Rad	Age	Error	Irrad.	*J*	Ar40	Ar40 Moles
20142-05	4.48959	0.0168	0.0034	3.4511	76.9	5.62	0.03	m2	0.0008743	0.0715	8.80E-16
20142-06	5.39046	0.7355	0.0070	3.3621	62.3	5.49	0.13	m2	0.0008743	0.0162	1.40E-16
20152-01	6.37733	0.0492	0.0092	3.6459	57.2	5.37	0.04	m2	0.0008743	0.1133	1.41E-15
20152-03	6.37815	1.0639	0.0087	3.8969	61.0	5.37	0.04	m2	0.0008743	0.0350	3.00E-16
20152-04	7.34648	1.3609	0.0093	4.7151	64.1	5.23	0.17	m2	0.0008743	0.0316	2.70E-16
20152-05	11.4678	1.0559	0.0263	3.7720	32.9	5.78	0.31	m2	0.0008743	0.0184	2.20E-16
Tuff of Elkhorn Spring						*Ave. 5.52 ± 0.01 Ma*					
MCD-1 (Ririe Reservoir/ Meadow Creek Dugway)											
15576-03A	1.98721	0.20514	0.00307	3.8100	95.1	5.78	0.02	29D	0.0017001	0.7566	3.81E-14
15576-04A	1.91328	0.04941	0.00156	1.8730	97.0	5.68	0.03	29D	0.0017001	0.3579	1.87E-14
15576-05A	2.05819	0.10191	0.00271	1.5230	90.9	5.72	0.04	29D	0.0017001	0.3131	1.52E-14
15576-06A	1.90748	0.26641	0.00230	0.9180	96.5	5.63	0.06	29D	0.0017001	0.1749	9.18E-15
15576-07A	1.89765	0.34990	0.00308	0.5490	98.6	5.60	0.16	29D	0.0017001	0.1041	5.49E-15
15576-08A	1.89997	0.21087	0.00136	0.3610	96.4	5.63	0.24	29D	0.0017001	0.0684	3.61E-15
15576-12A	2.12303	0.35727	0.00250	0.2390	86.8	5.62	0.20	29D	0.0017001	0.0506	2.39E-15
15576-14A	1.95105	0.04620	0.00338	0.2950	94.2	5.62	0.20	29D	0.0017001	0.0575	2.95E-15
16109-03A	1.85562	0.05817	0.00017	1.8038	97.2	5.64	0.06	34C	0.0017373	0.1294	7.03E-15
16109-04A	2.14697	1.11169	0.00124	1.7760	82.7	5.55	0.70	34C	0.0017373	0.0137	7.72E-16
16109-05A	2.19905	1.00505	0.00150	1.7504	79.6	5.47	0.18	34C	0.0017373	0.0558	3.15E-15
						Ave. 5.73 ± 0.01 Ma					
WRWC (West Ririe Reservoir/ Wolverine Creek)											
20008-01	12.2259		0.0008	11.9815	98.1	5.94	0.07	1	0.0002638	0.0293	2.55E-15
20005-01	139972		0.0001	11.1842	80.0	5.89	0.10	1	0.0002638	0.0773	6.72E-15
20016-03	14.2675		0.0020	12.8756	90.3	6.03	0.09	1	0.0002638	0.0031	2.67E-16
20032-01	18.5432	0.0000	0.0203	12.519	67.5	5.88	0.15	1	0.0002638	0.1227	1.09E-14
20032-03	16.5755	4.5922	0.0156	12.333	74.1	5.94	0.65	1	0.0002638	0.0644	5.74E-15
20032-04	12.2214	2.6796	0.0034	11.416	93.2	5.54	0.64	1	0.0002638	0.0503	4.73E-15
20032-05	12.4479	4.6607	0.0045	11.504	92.0	5.59	0.61	1	0.0002638	0.0503	4.49E-15
20080-01	12.9533	0.0418	0.0037	11.846	91.5	5.81	0.13	LL1-A	0.0002590	0.0430	5.40E-16
20080-02	33.7925	0.9617	0.0736	12.100	35.8	5.91	0.30	LL1-A	0.0002590	0.0962	8.80E-16
20080-03	13.3994	0.8966	0.0085	10.969	81.8	5.86	0.12	LL1-A	0.0002590	0.0405	3.70E-16
20080-04	17.9904	1.0344	0.0234	11.152	61.9	5.93	0.11	LL1-A	0.0002590	0.0740	6.80E-16
20044-01	2.66455	0.9343	0.0016	2.2369	83.9	5.82	0.07	LL1-A	0.0002590	0.0857	7.90E-16
16104-01A	2.62214	0.8946	0.0032	1.6705	63.7	5.22	0.35	34C	0.0017373	0.0336	1.90E-15
16104-01B	1.85762	0.0349	0.0001	1.8121	97.6	5.66	0.19	34C	0.0017373	0.0416	2.35E-15
16104-02A	2.36500	0.9214	0.0022	1.7050	72.1	5.33	0.21	34C	0.0017373	0.0501	2.83E-15
16104-02B	2.12118	0.0389	0.0010	1.8665	85.6	5.68	0.05	34C	0.0017373	0.1837	1.04E-14
16104-03A	3.40754	1.1387	0.0052	1.8534	54.4	5.79	0.47	34C	0.0017373	0.0326	1.84E-15
16104-03B	2.11558	1.0032	0.0013	1.7224	81.4	5.38	0.27	34C	0.0017373	0.3099	1.88E-15
16104-04A	1.86794	0.0366	0.0002	1.8150	97.2	5.67	0.03	34C	0.0017373	0.3099	1.75E-14
16104-04B	2.12972	1.3561	0.0011	1.7717	83.2	5.54	0.38	34C	0.0017373	0.0244	1.38E-15
16104-05A	1.95829	0.0199	0.0007	1.9055	63.4	5.96	0.79	34C	0.0017373	0.0166	9.40A-16
16104-05B	1.88243	0.9855	0.0005	1.7354	92.2	5.43	0.17	34C	0.0017373	0.0473	2.67E-15
						Ave. 5.71 ± 0.03 Ma					
HEC (Heise Cliffs)											
12221-02	2.09890	1.1513	0.0032	1.2235	58.3	5.83	0.61		0.0026210	0.0075	1.05E-15
12221-04	2.01262	1.1278	0.0034	1.0749	58.3	5.57	0.46		0.0026210	0.0109	9.80E-14
12221-07	1.80010	0.7349	0.0021	1.2070	68.3	5.89	0.06		0.0026210	0.0933	1.31E-14
						Ave. 5.88 ± 0.06 Ma					
Tuff of Wolverine Creek						*Ave. 5.72 ± 0.01 Ma*					
TCC (Signal Mountain)											
20072-01	19.6115	0.9906	0.0265	11.611	60.4	5.93	0.24	LL1-A	0.0002590	0.0307	2.80E-16
20072-02	17.0494	0.9006	0.0144	12.8418	75.3	6.11	0.39	LL1-A	0.0002590	0.0123	1.10E-16
20072-04	16.7973	0.9474	0.0199	10.9749	65.3	5.87	0.23	LL1-A	0.0002590	0.0171	2.10E-16
20073-02	15.0629	0.9850	0.0099	12.2051	81.0	6.11	0.20	LL1-A	0.0002590	0.0186	1.70E-16
20042-02	3.69459	1.0430	0.0048	2.3292	63.0	6.06	0.21	6	0.0013800	0.0341	3.20E-16
20042-03	3.06932	1.1161	0.0026	2.3795	77.5	5.96	0.14	6	0.0013800	0.0417	3.80E-16
20042-04	3.45687	1.0780	0.0034	2.5150	72.7	6.06	0.19	6	0.0013800	0.0350	4.40E-16
20042-05	2.91714	1.1294	0.0018	3.4566	84.1	6.05	0.18	6	0.0013800	0.0237	2.20E-16

Table 1. (continued)

Sample	40/39	37/39	36/39	40*/39	%Rad	Age	Error	Irrad.	*J*	Ar40	Ar40 Moles
Conant Creek Tuff						*Ave. 6.01 ± 0.07 Ma*					
HER (S. Lemhi Range, N. Snake River Plain)											
20058-01	3.43803	1.2925	0.0024	2.7991	81.3	6.46	0.15	6	0.0013800	0.2241	2.06E-15
20058-06	3.72611	1.3206	0.0040	2.6196	70.2	6.31	0.09	6	0.0013800	0.0637	8.00E-16
20058-07	3.76767	1.3074	0.0040	2.6570	70.4	6.07	0.12	6	0.0013800	0.0908	8.40E-16
15578-07A	2.72231	2.69062	0.00182	0.1170	76.7	6.39	0.51	29D	0.0017001	0.0318	1.17E-15
15578-09A	2.61437	2.21756	0.00586	0.0420	80.5	6.44	1.41	29D	0.0017001	0.0109	1.09E-15
15578-11A	2.62561	0.15010	0.00227	0.0900	79.8	6.41	0.65				
						Ave. 6.27 ± 0.07 Ma					
WTAF (American Falls, S. Snake River Plain)											
20057-01	3.39493	0.9958	0.0024	2.7557	81.1	6.40	0.09	6	0.0013800	0.2705	3.39E-15
20057-04	3.14862	1.0586	0.0023	2.5431	80.7	6.13	0.10	6	0.0013800	0.0583	5.40E-16
20057-05	3.00847	1.2930	0.0031	2.1843	72.5	5.68	0.43	6	0.0013800	0.0177	2.20E-16
20057-06	5.05772	1.0984	0.0095	2.3155	45.7	6.28	0.34	6	0.0013800	0.0369	3.40E-16
20057-07	6.42790	1.0912	0.0132	2.5826	40.1	6.24	0.16	6	0.0013800	0.2418	2.23E-15
						Ave. 6.27 ± 0.05 Ma					
Walcott Tuff						*Ave. 6.27 ± 0.01 Ma*					
SL1 (Southern Lost River Range)											
20050-01	3.33117	0.0629	0.0017	2.7998	84.0	6.74	0.05	6	0.0013800	1.9732	2.48E-14
20050-02	2.77155	0.0274	0.0002	2.7141	97.9	6.62	0.03	6	0.0013800	3.8309	3.53E-14
20050-03	2.89191	0.0464	0.0005	2.7409	94.8	6.60	0.03	6	0.0013800	1.4754	1.36E-14
20050-04	2.82660	0.0283	0.0003	2.7453	97.1	6.62	0.03	6	0.0013800	1.3556	1.25E-14
						Ave. 6.63 ± 0.02 Ma					
DR98-44B (Blackfoot, Idaho)											
20090-02	4.33534	0.0183	0.0010	4.0458	93.3	6.74	0.03	M2	0.0009700	1.0575	9.00E-15
20090-03	4.31338	0.0180	0.0011	3.9722	92.1	6.65	0.01	M2	0.0009700	1.0743	1.34E-14
20090-04	4.20040	0.0179	0.0006	4.0187	95.7	6.68	0.03	M2	0.0009700	0.6258	5.33E-15
						Ave. 6.66 ± 0.01 Ma					
HCB (Heise Cliffs)											
20004-05	14.9380		0.0023	14.252	95.5	6.66	0.04	1	0.0002638	1.1739	1.73E-13
20007-05	14.0034		0.0013	13.605	97.2	6.66	0.04	1	0.0002638	0.0927	1.00E-14
20010-05	14.8304		0.0024	14.118	95.3	6.80	0.07	1	0.0002638	0.0612	6.61E-15
20028-01	13.3271	0.0005	0.0000	13.170	98.8	6.65	0.02	1	0.0002638	1.3273	1.18E-13
20054-01	2.92701	0.2543	0.0007	2.7180	93.1	6.67	0.04	6	0.0013800	3.7274	4.48E-14
						Ave. 6.66 ± 0.02 Ma					
SCB-1 (Snaky Canyon, S. Beaverhead Mountains)											
15574-04A	2.29054	0.0564	0.0027	1.3500	96.4	6.75	0.05	29D	0.0017001	0.3089	3.09E-14
15574-05A	2.39743	0.0576	0.0039	0.5580	90.0	6.60	0.11	29D	0.0017001	0.1336	1.34E-14
15574-06A	2.51622	0.0479	0.0032	0.5100	85.2	6.55	0.12	29D	0.0017001	0.1283	1.28E-14
15574-07A	2.43834	0.0493	0.0028	0.9490	90.2	6.72	0.06	29D	0.0017001	0.2312	2.31E-14
15574-08A	2.50271	0.0499	0.0025	1.5060	87.6	6.71	0.04	29D	0.0017001	0.3768	3.77E-14
15574-09A	2.39879	0.0511	0.0511	0.7450	91.4	6.70	0.08	29D	0.0017001	0.1787	1.79E-14
16101-01A	2.17404	0.0240	0.0001	2.1511	98.9	6.72	0.05	34C	0.0017373	1.1999	1.14E-14
16101-02A	2.21289	0.0235	0.0004	2.1072	95.2	6.59	0.03	34C	0.0017373	0.5826	3.29E-14
16101-01B	2.37893	0.0234	0.0009	2.1078	88.6	6.59	0.09	34C	0.0017373	0.2543	1.44E-14
						Ave. 6.66 ± 0.02 Ma					
8 T001 (W. Ririe Reservoir)											
15572-03A	2.21365	0.0521	0.0002	2.3530	98.5	6.67	0.03	29D	0.0017001	0.5206	5.12E-14
15572-04A	2.21952	0.0510	0.0024	2.0430	98.0	6.65	0.03	29D	0.0017001	0.4531	4.54E-14
15572-07A	2.33841	0.0530	0.0029	1.7830	92.8	6.63	0.04	29D	0.0017001	0.4165	4.17E-14
15572-08A	2.43205	0.0503	0.0031	1.6010	88.9	6.62	0.04	29D	0.0017001	0.3890	3.89E-14
15572-09A	2.23081	0.0524	0.0022	1.3760	98.7	6.73	0.05	29D	0.0017001	0.3067	3.07E-14
15572-11A	2.23960	0.0513	0.0022	2.6780	97.4	6.67	0.02	29D	0.0017001	0.5995	6.00E-14
15572-12A	2.20086	0.0520	0.0028	1.9560	98.4	6.63	0.03	29D	0.0017001	0.4302	1.96E-14
15572-13A	2.34206	0.0504	0.0034	1.1300	98.6	6.74	0.05	29D	0.0017001	0.2523	2.52E-14
						Ave. 6.66 ± 0.01 Ma					
Blacktail Creek Tuff						*Ave. 6.66 ± 0.01 Ma*					

Table 2. Picabo Volcanic Field Ignimbrites $^{39}Ar/^{40}Ar$ Isotopic Ages

Sample	40/39	37/39	36/39	40*/39	%Rad	Age	Error	Irrad.	*J*	Ar40	Ar40 Moles
HL86 (American Falls)											
20062-01	3.7691	0.0373	0.0020	3.1523	83.6	7.61	0.03	6	0.0001380	2.3190	2.14E-14
20062-02	3.4945	0.0421	0.0011	3.1447	90.0	7.59	0.02	6	0.0001380	2.9046	3.64E-14
20062-03	3.7298	1.3022	0.0022	3.1485	84.3	7.59	0.05	6	0.0001380	0.3081	2.84E-15
20062-05	3.3369	0.0420	0.0008	3.0946	92.7	7.57	0.02	6	0.0001380	3.1469	2.79E-14
Tuff of American Falls						*Ave. 7.58 ± 0.01 Ma*					
HPER-2 (Howe Point)											
20011-02	25.715	0.0000	0.0324	13.495	68.9	8.86	0.98	1	0.0002638	0.0798	6.80E-16
20008-02	52.838	0.0000	0.1134	19.307	36.5	8.87	0.55	1	0.0002638	0.0131	1.57E-15
20034-01	19.726	0.0000	0.0043	18.433	93.5	8.88	0.57	1	0.0002638	0.0954	1.16E-14
Three samples below not used											
20034-02	34.851	0.0000	0.0435	47.701	137	22.85	2.80	1	0.0002638	0.0457	8.27E-15
20034-03	18.540	0.0000	0.0081	20.933	112	10.06	0.80	1	0.0002638	0.0511	4.55E-15
20034-04	19.074	0.0000	0.0056	20.743	109	9.97	0.68	1	0.0002638	0.0769	6.85E-15
Tuff of Lost River Sinks						*Ave. 8.87 ± 0.16 Ma*					
NHPKC-1 (N. Howe Point)											
20087-02	5.7917	0.0168	0.0006	5.5898	96.5	9.34	0.04	M2	0.0009700	0.8215	2.23E-14
20087-03	5.7388	0.0236	0.0005	5.5604	96.9	9.29	0.04	M2	0.0009700	0.9438	1.03E-14
20087-04	5.6188	0.0206	0.0002	5.5616	99.0	9.30	0.04	M2	0.0009700	0.9054	8.03E-15
20087-05	5.6278	0.0176	0.0002	5.5646	98.9	9.30	0.03	M2	0.0009700	1.7241	2.07E-14
20087-06	5.6537	0.0183	0.0002	5.5948	99.0	9.35	0.03	M2	0.0009700	1.1336	1.47E-14
20087-07	5.6472	0.0212	0.0004	5.5851	97.5	9.20	0.03	M2	0.0009700	0.7948	1.42E-14
						Ave. 9.29 ± 0.01 Ma					
WAMR-1 (West of Arco)											
20088-01	5.5970	0.0216	0.0003	5.5169	98.6	9.22	0.03	M2	0.0009700	2.2999	2.55E-14
20088-02	5.6037	0.0225	0.0002	5.5387	98.8	9.26	0.02	M2	0.0009700	2.2877	1.95E-14
20088-03	5.6035	0.0226	0.0001	5.5568	99.1	9.29	0.03	M2	0.0009700	1.0789	1.35E-14
20088-04	5.5878	0.0294	0.0001	5.5744	99.6	9.32	0.03	M2	0.0009700	1.7757	1.51E-14
20088-05	5.6382	0.0255	0.0004	5.5080	97.7	9.22	0.03	M2	0.0009700	1.1759	1.00E-14
20088-06	5.6173	0.0291	0.0002	5.5417	98.7	9.26	0.03	M2	0.0009700	1.2160	1.02E-14
20088-07	5.6421	0.0181	0.0003	5.5431	98.2	9.28	0.02	M2	0.0009700	2.1695	2.71E-14
						Ave. 9.27 ± 0.01 Ma					
Tuff of Kyle Canyon						*Ave. 9.28 ± 0.01 Ma*					
WAER-1 (west of Arco)											
20009-04	20.205	0.0000	0.0018	20.227	99.6	9.59	0.05	1	0.0002638	0.0036	3.20E-15
20013-01	21.251	0.0000	0.0039	20.628	94.8	9.67	0.07	1	0.0002638	0.0971	1.24E-14
20036-01	20.290	1.1171	0.0507	18.888	93.0	9.09	0.05	1	0.0002638	0.5659	5.04E-14
20036-02	19.908	0.0000	0.0016	19.408	98.3	9.58	0.05	1	0.0002638	0.4154	5.04E-14
Tuff of Little Chokecherry Canyon (West of Arco)						*Ave. 9.46 ± 0.03 Ma*					
AVFH-1 (Fort Hall)											
20003-04	23.487	0.0000	0.0065	21.558	91.8	10.29	0.05	1	0.0002638	1.1170	9.95E-14
20015-01	24.038	0.0000	0.0086	21.369	89.4	10.27	0.08	1	0.0002638	0.0594	3.36E-15
HPAV-1 (Howe Point)											
20161-01	6.4152	0.0153	0.0002	7.2874	99.1	10.18	0.03	m2	0.0008800	2.6529	2.25E-14
20161-05	6.3992	0.0115	0.0004	6.3992	98.2	10.20	0.03	m2	0.0008800	5.1700	4.38E-14
20146-03	7.1847	2.3136	0.0033	7.1847	88.4	10.20	0.03	m2	0.0008800	0.4666	5.84E-14
LRAV-1 (S. Lost River Range)											
20048-05	4.3857	0.1932	0.0004	4.2682	97.3	10.26	0.03	6	0.0001380	2.4667	2.26E-14
20048-06	4.3307	0.0184	0.0003	4.2374	97.8	10.22	0.03	6	0.0001380	3.0025	2.77E-14
Arbon Valley Tuff B						*Ave. 10.22 ± 0.01*					
AVFH-1 (Fort Hall)											
20037-01	22.617	0.1130	0.0022	21.954	97.1	10.43	0.05	1	0.0002638	0.8689	7.74E-14
20037-02	22.871	0.0324	0.0018	22.326	97.6	10.37	0.05	1	0.0002638	0.7933	7.06E-14
20037-03	22.312	0.0000	0.0012	21.929	98.3	10.34	0.05	1	0.0002638	0.4963	6.02E-14

Table 2. (continued)

Sample	40/39	37/39	36/39	40*/39	%Rad	Age	Error	Irrad.	J	Ar40	Ar40 Moles
HPAV-1 (Howe Point)											
20161-03	6.5623	0.0102	0.0005	6.4203	97.8	10.42	0.02	m2	0.0008800	2.3376	2.91E-14
20161-04	6.7823	0.0127	0.0013	6.3896	94.2	10.38	0.03	m2	0.0008800	2.0338	1.72E-14
LRAV-1 (S. Lost River Range)											
20048-02	5.0600	0.0166	0.0024	4.3394	85.8	10.44	0.04	6	0.0001380	10.200	9.40E-14
20048-07	4.8745	2.4345	0.0022	4.3962	90.0	10.44	0.07	6	0.0001380	0.0287	3.60E-15
Arbon Valley Tuff A					*Ave. 10.41 ± 0.01*						

successive melts of hydrothermally altered rock [cf. *Boroughs et al*., 2005]. A similar conclusion was reached by *Watts et al*. [2011] for the Heise volcanic field including the 6.66 Ma Blacktail Creek Tuff, the 5.72 Ma tuff of Wolverine Creek, and the last eruption of the Heise Volcanics, the 4.61 Ma Kilgore Tuff. Microprobe analysis of glasses from ashfall tuff deposits from the Picabo and Heise volcanic fields show a general trend in the iron/titanium ratios with an increase from older ashfall tuff to the first ashfall tuff from the Heise volcanic field eruptions [*Anders et al*., 2009]. The analysis of feldspar major element chemistry we have undertaken yield some slight differences between the various ignimbrites within WO-2 thus allowing us to place some limits on correlations amongst ignimbrites found in outcrops along the margins of the eastern Snake River Plain.

4. Results

4.1. Single-Crystal Laser Fusion $^{40}Ar/^{39}Ar$ Isotopic Analysis

We analyzed 181 sanidine and plagioclase feldspars grains from 29 outcrops of the Heise and Picabo volcanic fields for $^{40}Ar/^{39}Ar$ age determinations (Tables 1 and 2). Six samples from the Heise volcanic field were step heated for comparison purposes (supporting information Figure S1). We also analyzed 65 individual feldspar grains from 12 samples recovered from the WO-2 core (Table 3). For WO-2 samples, each age determination was made from feldspars recovered from a 2.54 cm diameter perpendicular core of the main recovered core. We removed from the age determination a total of 11 samples from WO-2 due to highly discordant ages and/or low radiogenic ^{40}Ar.

The uppermost ignimbrite in WO-2 is poorly welded and contains many lithic and pumice fragments with a very low percentage of feldspars. The mean age for the two feldspars used is 5.45 ± 0.05 Ma. The large difference between the two ages (5.19 ± 0.09 Ma and 5.56 ± 0.06 Ma) is likely due to the low radiogenic ^{40}Ar yield, especially for the 5.19 Ma sample. However, the combined error overlaps with the 5.52 ± 0.01 Ma age of the tuff of Elkhorn Spring from the Heise Cliffs (Table 1). So given its stratigraphic position in the WO-2 core, age, and similar petrographic characteristics, we correlate the uppermost ignimbrite in WO-2 to the tuff of Elkhorn Spring (Figure 3).

The next major ignimbrite unit below the tuff of Elkhorn Spring in WO-2 did not yield a $^{40}Ar/^{39}Ar$ age. This unit is tuffaceous and feldspar poor. The base of this unit is marked by ~2 m thick surge deposit. Due to its stratigraphic position between the tuff of Elkhorn Spring above it and the age of the unit below it, this 4.3 m thick unit is correlated to the 5.72 ± 0.03 Ma tuff of Wolverine Creek. Petrographic examination reveals millimeter-scale round obsidian balls and vitric shards; though not unique to ignimbrites, both are similar to those observed in outcrops of the tuff of Wolverine Creek. The ignimbrite unit below the surge deposit of the tuff of Wolverine Creek is poorly lithified and contains similar intermixed surge and tan tuffaceous sands (Figure 3). The $^{40}Ar/^{39}Ar$ dating of WO-2-3802 (Table 3) of this ignimbrite unit yields an age of 6.01 ± 0.01 Ma coeval with the Conant Creek Tuff at Signal Mountain dated at 6.01 ± 0.07 Ma (Table 2). Both these units at their respective sampling sites have very low (<1%) feldspar content with plagioclase making up the bulk of the feldspar content. Therefore, based on the identical ages, similar feldspar composition, and stratigraphic position within WO-2, we correlated it with the Conant Creek Tuff (Figure 2).

The next major unit below the Conant Creek Tuff is a massive rhyolite lava or series of lavas we named the rhyolite of Upper WO-2. Dates at two depth intervals (Table 3) yield a combined age of 6.21 ± 0.02 Ma. Below this unit is a 2 m thick ignimbrite, dated as 6.23 ± 0.14 Ma, which we called the tuff of WO-2. We know of no exposed rocks that correlate to either the lava or the ignimbrite unit.

Table 3. WO-2 $^{39}Ar/^{40}Ar$ Isotopic Ages[a]

Sample	40/39	37/39	36/39	40*/39	%Rad	Age	Error	Irrad.	J	Ar40	Ar40 Moles
WO2-3762[a]											
6647-04A	23.6969	0.5795	0.0543	7.6996	32.5	5.19	0.09	92A	0.0003697	5.8072	2.57E-14
6647-05A	18.1182	0.8616	0.0337	8.2270	45.4	5.56	0.06	92A	0.0003697	5.6716	2.30E-14
Samples below not used											
6647-02A	22.9074	0.8076	0.0582	5.7783	25.2	3.91	0.09	92A	0.0003697	3.9671	2.02E-14
6647-01A	10.6295	0.4975	0.0049	9.2252	86.8	6.18	0.02	92A	0.0003697	2.2206	1.16E-14
6647-03A	33.2456	0.8476	0.1037	2.6534	8.0	1.78	0.13	92A	0.0003697	10.0585	4.60E-14
Tuff of Elkhorn Spring (5.52 ± 0.01 Ma)						*Ave. 5.45 ± 0.05 Ma*					
WO2-3802											
20086-02	3.9378	0.0160	0.0011	3.5908	91.5	6.01	0.03	M2	0.0009700	1.0518	6.72E-15
20086-03	3.6893	0.0138	0.0003	3.5884	97.5	6.00	0.02	M2	0.0009700	1.5640	1.33E-14
20086-04	3.9197	0.0162	0.0010	3.5971	92.2	5.97	0.01	M2	0.0009700	1.0518	8.95E-15
20086-05	3.6374	0.0151	0.0002	3.5727	98.5	6.03	0.02	M2	0.0009700	0.6622	8.27E-15
20086-06	3.8768	0.0149	0.0008	3.6177	93.6	6.02	0.02	M2	0.0009700	0.8995	7.66E-15
20086-07	3.9078	0.0174	0.0010	3.5970	92.3	6.02	0.07	M2	0.0009700	0.1877	1.66E-15
10873-01	1.4328	0.0242	0.0001	1.4046	98.0	5.52	0.10	21	0.0022930	0.2038	
10873-02	1.4733	0.0252	0.0004	1.3615	92.4	5.98	0.06	21	0.0022930	0.1652	
10873-03	1.5253	0.0244	0.0002	1.4477	94.9	6.03	0.04	21	0.0022930	0.1348	
10873-04	1.4614	0.0264	0.0001	1.4414	98.9	6.09	0.03	21	0.0022930	0.2387	
10873-05	1.5773	0.0266	0.0005	1.4278	90.5	6.10	0.03	21	0.0022930	0.1336	
10873-06	1.4303	0.0260	0.0001	1.4167	99.1	5.74	0.04	21	0.0022930	0.0785	
10873-07	1.4658	0.0246	0.0005	1.3069	89.2	5.92	0.03	21	0.0022930	0.0467	
Conant Creek Tuff (6.01 ± 0.01 Ma)						*Ave. 6.01 ± 0.01 Ma*					
WO2-3834											
6649-03	12.3431	1.8845	0.0106	9.3793	75.9	6.32	0.03	92A	0.0003697	0.6634	3.18E-15
6649-04	9.9262	1.8633	0.0026	9.3176	93.8	6.28	0.03	92A	0.0003697	0.4421	2.19E-15
6649-05	13.4391	1.6116	0.0142	9.3692	69.7	6.32	0.03	92A	0.0003697	0.9054	4.53E-15
6649-01	15.1470	1.1581	0.0206	9.1527	60.4	6.17	0.04	92A	0.0003697	1.0353	5.09E-15
Sample below not used											
6649-02	14.5060	2.2379	0.0147	10.3439	71.2	6.93	0.04	92A	0.0003697	0.6689	3.42E-15
WO2-4132											
6651-01A	11.1431	0.7834	0.0072	9.0728	81.4	6.12	0.03	92A	0.0003697	2.4539	1.11E-14
6651-05	11.9536	0.3444	0.0092	9.2643	77.5	6.25	0.03	92A	0.0003697	4.5979	1.98E-14
6651-02A	13.1494	2.0006	0.0150	8.8748	67.4	5.99	0.03	92A	0.0003697	0.7684	4.17E-15
Samples below not used											
6651-03A	10.2225	1.9611	0.0022	9.7276	95.1	6.52	0.02	92A	0.0003697	0.4451	2.09E-15
6651-04A	11.1563	2.2535	0.0048	9.9355	89.0	6.65	0.03	92A	0.0003697	0.4809	2.37E-15
Rhyolite of Upper WO-2						*Ave. 6.21 ± 0.02 Ma*					
WO2-4155											
20096-01	5.9181	0.7560	0.0083	3.4990	59.1	6.19	0.26	M2	0.0009700	0.1194	1.68E-15
20096-02	5.7405	0.9127	0.0077	3.5428	61.7	6.27	0.26	M2	0.0009700	0.0914	7.80E-16
20096-03	6.8012	0.8842	0.0111	3.5577	52.3	6.29	0.21	M2	0.0009700	0.0785	6.70E-16
Tuff of WO-2						*Ave. = 6.23 ± 0.14 Ma*					
WO2-4250											
20052-04	4.1772	1.2344	0.0057	2.5612	61.3	6.18	0.08	6	0.0013800	0.3156	3.96E-15
20052-06	3.7916	0.8583	0.0045	2.4927	65.7	6.33	0.06	6	0.0013800	0.1773	1.51E-15
20051-07	4.3214	1.1982	0.0060	2.6192	60.5	6.27	0.14	6	0.0013800	0.4971	2.20E-15
Samples below not used											
20052-02	6.8226	2.2143	0.0090	4.3189	63.2	10.34	0.02	6	0.0013800	0.1276	1.18E-15
20052-01	10.6879	1.9059	0.0282	0.0909	26.4	6.23	0.34	6	0.0013800	0.6730	8.40E-15
20052-03	6.1580	1.2390	0.0116	2.7928	45.3	6.77	0.13	6	0.0013800	0.1347	2.20E-15
WO2-4254											
6653-01	17.5749	1.3252	0.0291	9.0962	51.7	6.17	0.05	92A	0.0003697	1.3931	7.30E-15
6653-02	16.8829	1.1904	0.0263	9.2025	54.5	6.25	0.04	92A	0.0003697	1.2997	6.61E-15
6653-03	14.2123	1.2028	0.0167	9.3601	65.8	6.35	0.04	92A	0.0003697	0.6730	3.14E-15
6653-04	11.6185	1.1407	0.0085	9.2050	79.2	6.25	0.03	92A	0.0003697	0.4971	2.20E-15
Sample below not used											
6653-05	10.1657	0.2598	0.0021	9.5589	94.1	6.47	0.02	92A	0.0003697	1.8387	9.24E-15

Table 3. (continued)

Sample	40/39	37/39	36/39	40*/39	%Rad	Age	Error	Irrad.	J	Ar40	Ar40 Moles
Walcott Tuff A (6.27 ± 0.01 Ma)						*Ave. 6.26 ± 0.02 Ma*					
WO2-4340											
6657-01	10.2456	0.4391	0.0022	9.6156	93.9	6.44	0.02	92A	0.0003697	1.9772	9.85E-15
6657-02	10.3983	0.2460	0.0028	9.5736	92.1	6.41	0.02	92A	0.0003697	2.0104	9.45E-15
6657-04	13.7854	0.2362	0.0145	9.5078	69.0	6.37	0.04	92A	0.0003697	3.5928	1.79E-14
6657-05	18.7889	0.5928	0.0325	9.2225	49.1	6.18	0.06	92A	0.0003697	2.6217	1.42E-14
Sample below not used											
6657-03	11.7709	0.4490	0.0061	10.0102	85.1	6.74	0.02	92A	0.0003697	2.0893	9.85E-15
WO2-4543											
6654-01	10.5599	0.1773	0.0033	9.5945	90.9	6.43	0.02	92A	0.0003697	1.7703	8.69E-15
6645-02	10.7378	0.3361	0.0045	9.4206	87.8	6.31	0.02	92A	0.0003697	1.0549	5.38E-15
6654-03A	10.2189	0.1858	0.0021	9.6095	94.1	6.44	0.02	92A	0.0003697	1.4017	6.73E-15
6654-04A	10.3580	0.1982	0.0026	9.5935	92.7	6.43	0.02	92A	0.0003697	1.1536	5.60E-15
6654-05A	9.9096	0.1910	0.0013	9.5497	96.4	6.40	0.02	92A	0.0003697	1.2282	5.77E-15
WO2-4932											
6660-01	11.2404	0.2337	0.0053	9.6804	86.1	6.49	0.02	92A	0.0003697	2.5219	1.27E-14
6660-02	11.3612	0.3711	0.0057	9.6959	85.4	6.50	0.02	92A	0.0003697	1.1430	5.63E-15
6660-03	11.2199	0.1061	0.0054	9.6229	85.8	6.45	0.02	92A	0.0003697	2.4657	1.18E-14
6660-04	11.8781	0.5452	0.0082	9.4981	80.0	6.36	0.02	92A	0.0003697	1.1203	5.45E-15
6660-05	11.0448	0.1273	0.0050	9.5825	86.8	6.42	0.02	92A	0.0003697	1.6485	7.97E-15
Rhyolite of Lower WO-2						*Ave. 6.45 ± 0.01 Ma*					
WO2-4940.6											
20003-1	26.4923	0.1360	0.0048	13.769	52.0	6.57	0.07	1	0.0002638	1.3093	1.14E-13
20017-2	18.9625	0.0096	0.0180	13.564	71.6	6.68	0.06	1	0.0002638	0.0707	8.39E-15
20014-1	15.9462	0.0001	0.0062	14.082	88.4	6.76	0.08	1	0.0002638	0.0291	2.54E-14
WO2-4998.8											
20009-5	16.9820	0.01	0.0053	13.917	81.8	6.62	0.04	1	0.0002638	2.5219	7.11E-15
20003-5	15.6105	0.05	0.0058	9.6959	89.1	6.64	0.03	1	0.0002638	1.2887	1.15E-13
20001-1	26.5508	0.04	0.0044	13.139	49.5	6.67	0.09	1	0.0002638	2.2870	1.99E-13
20018-1	15.3724	0.04	0.0048	13.918	90.6	6.69	0.05	1	0.0002638	0.0594	5.16E-15
10880-01	1.79673	0.0302	0.0007	1.5696	87.4	6.66	0.03	21	0.0022930	0.2416	1.86E-15
Blacktail Creek Tuff (6.66 ± 0.01 Ma)						*Ave. 6.65 ± 0.02 Ma*					

[a]Numbers following the WO2 designation are the depth from the surface in feet in borehole WO-2 (see Figure 3).

The next major unit below the tuff of WO-2 is a 26.8 m thick ignimbrite unit that is crystal poor, eutaxitic, and densely welded. We did not successfully date this tuff, but as discussed later its stratigraphic position and textural similarity to surface outcrops provide evidence it is the Walcott Tuff B. The ignimbrite is underlain by a 2.4 m thick ashfall tuff bed and then a 3.3 m thick ignimbrite, with a distinctive orange and black pattern of

Table 4. Argon-39/Argon-40 and U/Pb Isotopic Age Comparison[a]

Units	This StudyAr/Ar in Ma	Morgan and McIntosh(2005)[n] Ar/Ar in Ma	*Drew et al.* [2013] U/Pb in Ma[q]
Ignimbrites (*Heise*)			
Kilgore Tuff	4.61 ± 0.01 (43/7)[b]	4.51 ± 0.05 (72/6)	
Tuff of Elkhorn Spring	5.52 ± 0.01 (8/1)	5.55 ± 0.13 (7/1)	
Tuff of Wolverine Creek	5.72 ± 0.03 (33/2)	5.67 ± 0.05 (15/1)[o]	
Conant Creek Tuff	6.01 ± 0.07 (8/1)	5.70 ± 0.04 (2/2)[m]	
Tuff of WO-2 (in core only)	6.23 ± 0.14 (3/1)		
Walcott Tuff B	6.27 ± 0.01 (5/1)	6.35 ± 0.03 (2/2)[m]	
Walcott Tuff A (WO-2)	6.26 ± 0.02 (7/1)		
Blacktail Creek Tuff	6.66 ± 0.01 (23/5)	6.71 ± 0.03 (74/4)	
Ignimbrites (*Picabo*)			
Tuff of American Falls	7.58 ± 0.01 (4/1)		7.91 ± 0.16 (16/1)
Tuff of the Lost River Sinks	8.87 ± 0.16 (3/1)		7.05 ± 0.13 (15/1)
Tuff of Kyle Canyon[n]	9.28 ± 0.01 (13/2)		
Tuff of Little Chokecherry Canyon	9.46 ± 0.03 (4/1)[p]		9.7 ± 0.12[p] (12/1)

Table 4. (continued)

Units	This StudyAr/Ar in Ma	Morgan and McIntosh(2005)[n] Ar/Ar in Ma	*Drew et al*. [2013] U/Pb in Ma[q]
Arbon Valley Tuff B	10.22 ± 0.01 (7/3)		10.44 ± 0.27 (18/1)
Arbon Valley Tuff A	10.41 ± 0.01 (8/3)		
Arbon Valley Tuff (A and B)[j]	10.27 ± 0.01 (15/3)	10.34 ± 0.03 (91/6)[c]	
Rhyolite Lavas (*Heise*)			
Rhyolite of Reno Point	6.12 ± 0.02 (7/1)		
Rhyolite of Upper WO-2	6.21 ± 0.02 (7/2)		
Rhyolite of Lidy Hot Springs		6.28 ± 0.05	
Rhyolite of Lower WO-2	6.45 ± 0.02 (14/3)		
Rhyolite of Steven's Peak			6.62 ± 0.12 (13/1)
Rhyolite of Steven's Peak 2			6.86 ± 0.19[r] (14/1)
Rhyolite Lavas (*Picabo*)			
Rhyolite of Hawley Spring[i]		7.60 ± 0.04	
West Pocatello Rhyolite			8.25 ± 0.26[r] (15/1)
Ashfalls (*Heise*)			
Big Elk Creek Ash[g]	5.85 ± 0.04 (5/1)[d]	5.67 ± 0.07 (27/2)[f]	
Elkhorn Warm Springs Ash	5.85 ± 0.03 (5/1)[e]		
Little Elk Creek Ash[g]	7.00 ± 0.09 (3/1)[e]	6.63 ± 0.06 (15/1)[h]	
Ashfalls (*Picabo*)[i]			
Van Point Tephra 1	7.32 ± 0.04 (10/1)		
Phillips Ridge Ash[h]	7.36 ± 0.02 (6/1)		
Van Point Tephra 3	9.22 ± 0.06 (5/1)		
Colter Formation[k]	9.87 ± 0.14 (3/1)		
Van Point Ash 1	10.48 ± 0.02 (5/1)		
Basalts[l]			
Radio Tower Basalt[l]	4.21 ± 0.03 (1/1)		
Lone Pine Basalt[1]	7.08 ± 0.11 (1/1)		
Briggs Canyon Basalt[l]	7.56 ± 0.04 (1/1)		

[a]Data converted to a common standard age for the Fish Canyon Tuff of 28.201 Ma, uses $\lambda = 5.463E-10 \pm 1.07E-11$ and Noah McClean ArArReCalc 7/31/09; errors for *Morgan and McIntosh* [2005] are 2σ combining of analyses was done using *Taylor* [1982] statistics.

[b]Number in brackets represents the number of individual age determinations/number of sampling site;, errors are 1σ.

[c]Represents a combined age from sites in *Morgan and McIntosh* [2005]. All site means are converted as in footnote[a]. Result were merged using *Taylor* [1982] statistics.

[d]Based on stratigraphic position, mineralogy, physical characteristics, and age dating the Big Elk Creek and Elkhorn Warm Spring Ashes are the same unit and not correlative with the Conant Creek Tuff.

[e]The Elkhorn Warm Springs Ash is located in the Heise Cliffs, Idaho, between the tuff of Wolverine Creek and the tuff of Elkhorn Spring.

[f]Ages from two sampling sites (localities 11 and 12 in *Morgan and McIntosh* [2005]) combined using *Taylor* [1982] statistics.

[g]$^{39}Ar/^{40}Ar$ data from *Anders et al*. [2009] and *Anders* [1990] localities BEC and LEC.

[h]Andesitic ash underlying andesitic flow on Teton Pass road, labeled Tab in *Love et al*. [1992].

[i]Rhyolite flows and tephra deposits are grouped as Picabo based on age only.

[j]Grouping all Arbon Valley Tuff samples, assuming a single eruptive event.

[k]From *Anders et al*. [2009], Pilgrim Creek, Jackson Hole.

[l]From S. Lost River Range and Birch Creek Valleys, *Rodgers and Anders* [1990], *Anders et al*. [1993].

[m]Combined step-heating results from Hominy Peak site of *Morgan and McIntosh* [2005]. Applied *Taylor* [1982] statistics and standard correction Fish Canyon Tuff of 28.201 Ma—see footnote[a].

[n]A date of 9.91 ± 0.90 Ma on zircon (unclear technique used) is given in *McBroome* [1981].

[o]Samples from the east and west side of the Riere Reservoir.

[p]Same sampling site as *Snider* [1995] of $^{40}Ar/^{39}Ar$ 9.4 ± 0.04 Ma (monitor standard not given).

[q]Errors are 1 sigma.

[r]Described in *Kellogg et al*. [1994] as rhyolite flows and in *Drew et al*. [2013] as ignimbrites.

altered glass shards and fine-grained black obsidian matrix, which was dated at 6.26 ± 0.02 Ma (Table 1). As we will discuss below, we called this lower ignimbrite unit the Walcott Tuff A.

Below the Walcott Tuff is a thick rhyolite lava or series of lavas we dated at 6.41 ± 0.01 Ma and named the rhyolite of Lower WO-2. *Anders et al*. [1997] previously mistook part of this unit to be an ignimbrite and erroneously call it the tuff of Wolverine Creek. However, using a criterion based on those of *Manley and Fink* [1987] and *Henry and Wolff* [1992], the rhyolite was determined to be lava. A similar conclusion was reached by *McCurry and Rodgers* [2009] in their study of eastern Snake River Plain drill cores.

Table 5. Paleomagnetism of Heise and Picabo Volcanic Fields[a]

Units	Site/Unit Mean						Site Locations	
	Inclination	Declination	α_{95}	K	R	N	N, Lat	W, Long
			Ignimbrites (*Heise*)					
Kilgore Tuff[b]	**−50.4**	**173.5**	**7.7**					
Tuff of Elkhorn Spring[k]	**−46.4**	**158.0**	**2.8**	298		11	43.649	111.692
Tuff of Wolverine Creek							43.505	111.763
Conant Creek Tuff[c]	**−49.9**	**166.5**	**11.4**	35		6	44.040	110.918
Tuff of Inel (WO-2 only)							43.580	112.875
Walcott Tuff[b]	**77.2**	**203.5**	**8.9**					
Walcott Tuff	71.3	233.2	1.9	2166	5.00	5	42.776	112.876
Blacktail Creek Tuff[b]	**66.5**	**18.5**	**3.3**					
			Ignimbrites (*Picabo*)					
Tuff of American Falls							42.785	112.838
Tuff of the Lost River Sinks	69.0	2.5	2.9	191	16.91	17	43.805	112.844
Tuff of Kyle Canyon (Howe Pt.)	76.7	6.0	1.5	805	12.98	13	43.908	112.857
Tuff of Kyle Canyon (W of Arco)	73.5	359.2	5.7	53	12.78	13	43.590	113.513
Tuff of Little Chokecherry Canyon	71.9	5.8	3.4	96	18.81	14	43.588	113.525
Arbon Valley Tuff B								
Arbon Valley Tuff A[d]	**57.5**	**304.5**	**7.3**	59	7.90	8	42.777	112.656
			Rhyolite Lavas (*Heise*)					
Rhyolite of Reno Point	−30.1	184.3	3.0	31	12.61	13	44.019	112.778
Rhyolite of Upper WO-2[e]	−70.8						43.580	112.875
Rhyolite of Lidy Hot Springs[k]								
Rhyolite of Lower WO-2[e]	43.1						43.580	112.875
			Ashes (*Heise*)					
Big Elk Creek Ash[f]	−44.1	137.5	6.9	55	9.81	17	43.320	111.139
Elkhorn Warm Springs Ash							43.649	111.692
Little Elk Creek Ash[g]	57.0	23.8	7.3	48		13	43.317	111.163
			Airfalls (*Picabo*)					
Van Point Tephra 1							43.504	110.923
Phillips Ridge Ash[i]							43.504	110.923
Van Point Tephra 3							43.288	111.164
Van Point Ash 1	52.2	325.0	19.2	6		15	43.296	111.159
			Andesites (*Heise*)					
Calamity Point Andesite[h]	−72.1	131.3	3.4	18		5	43.332	111.207

[a]Bold inclination and declination values are for unit means, all nonbold are for site means. Unit means for the tuff of Arbon Valley, tuff of Elkhorn Spring, and Conant Creek Tuff are based on a structural correction for one sampling site.
[b]From *Anders et al.* [1993]
[c]From *Reynolds* [1975], tuff of Boone Creek. Corrected for 10° west tilt about N-S axis, In situ $I = -51.2$ $D = 178.6$
[d]Based on a basal vitrophyre site corrected for a 16° SW tilt correction about 350° axis.
[e]Lat/Long for borehole site. No declination as core was free to spin during recovery. Inclinations determined by measurement of combined data from contiguous sections of core.
[f]Corrected for a 22° northeast tilt on an tilt axis of 290°. In situ $I = -49.9$ $D = 115.5$. See *Anders et al.* [2009].
[g]Corrected for a 25° tilt about a 340° tilt axis. In situ $I = 65.9$, $D = 338.0$, See *Anders et al.* [2009].
[h]From *Anders et al.* [1989].
[i]Andesitic ash from directly below unit Tab of *Love et al.* [1992] on Teton Pass Road.
[j]From *Morgan and McIntosh* [2005].
[k]Because sampling site HCK (tuff of Heise in *Anders et al.* [1993] is directly above HCE (tuff of Elkhorn Spring), following the correction path for HCK to the unit mean orientation HCE will follow the same correction path thus defining the unit mean.

The rhyolite lava(s) are underlain by red clay (possibly fault generated) and then a 18.9 m thick ignimbrite (Figure 3). The ages we obtained from the upper (WO-2 4940.6) and lower (WO-2 4998.8) horizons of this unit are almost identical to the age of the Blacktail Creek Tuff we get from outcrops −6.65 ± 0.02 Ma in the core (Table 3) compared to 6.66 ± 0.01 Ma from outcrops (Table 1). This unit marks the base of WO-2. We did a limited number of step-heating analyses to check against our single-crystal laser ablation analyses. For example, Figure S1 shows two step-heating analyses of the Blacktail Creek Tuff from north of the Snake River Plain (SCB, Figure 2a) and from south of the Snake River Plain (HCB, Figure 2a). The errors overlap with our combined age determination shown in Table 4. Analysis of step heating of the Kilgore Tuff also yields identical ages compared to the single-crystal laser ablation values – 4.61 ± 0.01 Ma based on 43 analyses compared to 4.61 ± 0.07 Ma for step heating (Figure A1).

Table 6. Paleomagnetic Results from WO-2

Unit	Depth	Inclination	Declination	α95	R	K	Af/mT	Comments[b]
Tuff of Elkhorn Sp.	3760.7	−34.4	254.6	38.1	2.827	11.5	70	Unit mean:[c]*Anders et al.* [1993]
5.52 Ma	3760.8	−32.5	220.0				70	$I = -46.4°$, $D = 158.0°$
	3760.9	−58.9	272.0				70	WO-2 mean inclination: $I = -43.9°$
Conant Creek	3825.3	−35.0	316.9	67.1	2.551	4.4	50	Unit mean[a]: Reynolds 1975
Tuff 6.01 Ma	3825.5	−36.7	225.8				30	$I = -49.9°$, $D = 178.6°$
	3825.6	−49.5	228.2				30	WO-2 mean inclination $I = -49.3°$
Rhyolite of Upper	3835.6	−70.9	25.2	7.8	2.992	250	70	WO-2 mean inclination:
WO-2 6.21 Ma	3835.7	−69.7	14.0				50	$I = -70.8°$
	3835.8	−72.7	354.4				50	No known equivalent
	3889.0	−61.1	44.5	none			30	outside WO-2
	3889.1	−58.1	49.4				30	
	3894.8	−78.4	182.2	none			30	
	3965.4	−69.1	7.0	5.3	3.990	298	30	
	3964.6	−70.6	27.0				30	
	3964.8	−72.8	22.0				30	
	3965.8	−68.4	0.0				30	
	4125.2	−78.8	266.4	12.2	2.980	103	30	
	4125.4	−80.1	268.7				50	
	4128.6	−65.7	262.5				90	
	4145.3	−67.5	244.3	10.8	2.985	130	30	
	4145.5	−54.7	239.8				30	
	4145.7	−66.1	241.1				30	
Walcott Tuff B	4236.6	81.4	240.4	11.3	2.983	119	30	Unit mean: *Anders et al.* [1993]
6.27 Ma	4236.8	72.2	275.8				30	$I = 77.4°$, $D = 203.5°$
	4237.1	77.2	300.0				30	WO-2 mean inclination: $I = 77.8°$
Walcott Tuff A	4250.2	68.2	151.4	10.0	2.987	154	70	Site mean: American Falls
6.26 Ma	4250.4	72.2	182.4				30	$I = 71.3°$, $D = 233.2°$
	4251.2	73.2	183.4				70	WO-2 mean inclination: $I = 71.8°$
Rhyolite of Lower	4275.8	42.8	124.1	5.8	2.996	449	NRM	WO-2 mean inclination:
WO-2 6.45 Ma	4276.1	45.6	114.4				10	$I = 43.1°$
	4276.3	43.8	121.1				30	No known equivalent
	4343.0	46.8	141.2	9.9	2.987	157	50	outside WO-2
	4343.2	51.7	142.1				50	
	4343.4	39.0	143.6				50	
	4449.4	36.9	87.6	7.9	2.992	246	30	
	4449.6	45.1	95.3				30	
	4449.8	41.1	88.4				30	
	4549.6	43.7	149.4	38.5	2.823	11.3	50	
	4549.8	46.5	173.3				50	

From the margins of the eastern Snake River Plain, we sampled several ignimbrites that likely represent the Picabo volcanic field (Table 2). The youngest of these is the aerially restricted 7.58 ± 0.01 Ma tuff of American Falls located 1.5 km east of American Falls (Figure 2)—a younger age is shown in Table S1 in the supporting information of 7.0 ± 2.0 Ma based on fission-track analysis that we feel is too imprecise to consider it further. The tuff of American Falls has centimeter-sized pumice and lithic fragments in a densely welded matrix with abundant feldspars as evidence of proximal deposition. Two ignimbrites from Howe Point on the northern margin of the eastern Snake River Plain (Figure 2) were analyzed: the tuff of the Lost River Sinks yielded an age of 8.87 ± 0.16 Ma and the tuff of Kyle Canyon an age of 9.29 ± 0.01 (NHPKC-1, Table 2). An ignimbrite found west of Arco, Idaho, yielded an age of 9.27 ± 0.01 (WAMR-1, Table 2). In thin section and at the outcrop scale these two outcrops are remarkably similar. Both have thick pinkish to dark brown basal vitrophyres, similar abundant feldspar compositions, and similar paleomagnetic orientations. We therefore correlated these two outcrops and give a combined age of 9.28 ± 0.01 Ma. Another ignimbrite west of Arco, WAER-1 in *Anders et al*. [1993], was thought to be the Blacktail Creek Tuff, but when dated turned out to be much older. We dated this unit at 9.46 ± 0.03 Ma and tentatively correlated it to the more extensive tuff of Little Chokecherry Canyon a few kilometers to the north that is dated at 9.52 ± 0.04 Ma (corrected for a common Fish Canyon Tuff monitor standard from *Snider* [1995]).

Table 6. (continued)

Unit	Depth	Inclination	Declination	$\alpha 95$	R	K	Af/mT	Comments[b]
	4550.3	45.5	218.7				70	
	4681.7	49.1	288.0	6.5	2.994	357	50	
	4681.9	44.2	280.0				30	
	4682.0	46.6	289.4				30	
	4752.5	45.4	179.8	6.2	2.995	390	30	
	4752.7	46.3	171.5				30	
	4752.9	44.5	168.9				30	
	4825.2	49.2	299.8	5.8	2.996	461	50	
	4825.3	43.1	297.1				50	
	4825.4	48.9	301.6				70	
	4900.3	41.9	14.0	5.1	2.997	578	30	
	4900.5	39.4	12.9				30	
	4900.7	43.6	19.5				30	
	4930.1	20.0	184.4	11.6	2.983	115	90	
	4930.3	22.5	188.5				30	
	4930.4	23.4	173.1				30	
Blacktail Creek	4940.6	58.1	300.3	9.9	2.987	155	80	Unit mean: *Anders et al.* [1993]
Tuff 6.66 Ma	4940.7	63.2	308.7				30	$I = 66.5°$, $D = 18.5°$
	4945.8	66.3	322.2				30	WO-2 mean inclination:
	4998.5	67.1	314.5	4.4	2.997	777	30	$I = 66.0°$
	4998.6	69.4	318.3				30	
	4998.8	69.7	328.1				30	

[a]Corrected for a 10° eastward tilt of the Teton Range [see *Byrd et al.*, 1994; *Anders et al.*, 2009].
[b]All inclination values for WO-2 means are calculated using *Arason and Levi* [2010].
[c]Correction made by following the correction path for HCK (Kilgore Tuff) positioned directly above HCE (tuff of Elkhorn Spring) in *Anders et al.* [1993].

The oldest of the Picabo volcanic field is the Arbon Valley Tuff. Regionally, this unit is a poorly welded ignimbrite and one of the few eastern Snake River Plain ignimbrites to have significant biotite. We dated this unit both where it is densely welded and where it is poorly welded. *Morgan and McIntosh* [2005] reported a range of ages on individual samples spanning over a million years that they averaged to yield an age of

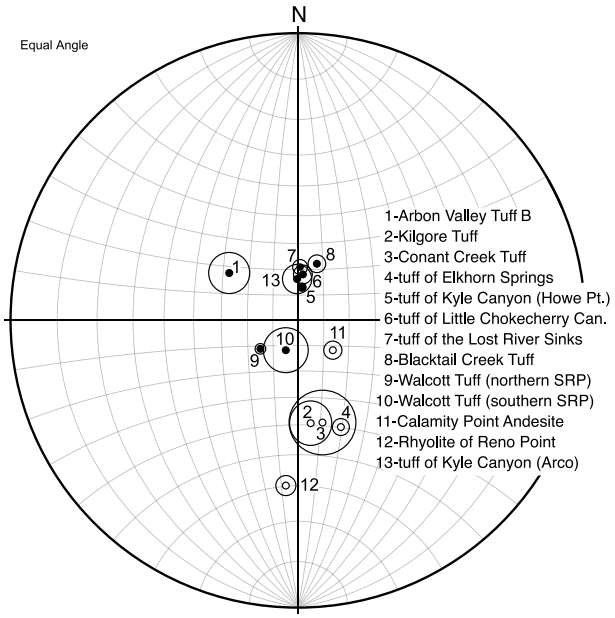

Figure 4. Paleomagnetism results from the eastern Snake River Plain volcanic rocks. Small open circles represent the upper hemisphere or reversed polarity. Small solid circle represent the lower hemisphere or normal polarity. Large circles surrounding smaller circles represent α_{95} confidence of *Fisher* [1953] statistics. The numeric values are provided in Table 5. Note that some data represent site means and others unit means.

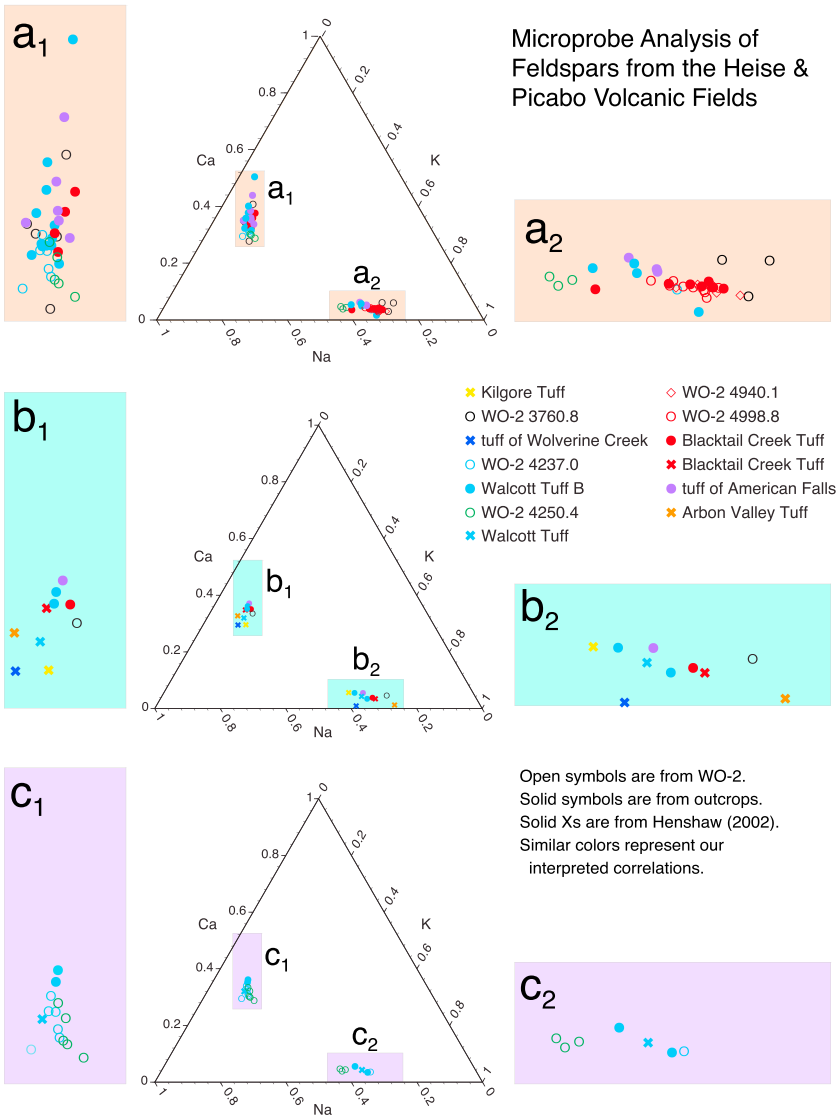

Figure 5. Ternary diagrams of major feldspar elemental composition. Enlarged areas of plagioclase feldspars are labeled Figures 5a1, 5b1, and 5c1. Enlarged areas of sanidine feldspars are labeled Figures 5a2, 5b2, and 5c2. Figure 5a represents all the geochemical data from this study. Solid circles represent outcrop data, and open symbols represent data from the WO-2 core. Figure 5b represents the averaged values for data from outcrops—the exception is the open black circle which is the averaged value from WO-2 core sample WO-2 3760.8. The solid crosses in Figure 5b are from the averaged values from microprobe study of feldspars from *Henshaw* [2002]. Note that the average value of WO-2 3760.8 does not match that of the Kilgore Tuff as determined by *Henshaw* [2002]. Figure 5c represents the averaged values of the Walcott Tuff from this study (solid blue circles) and the averaged value for the Walcott Tuff from *Henshaw* [2002] (solid cross). The Walcott Tuff data of Henshaw come from the American Falls area. Open circles represent data from WO-2 core with open blue circles representing WO-2 4237.0 and open green circles represent WO-2 4250.4 which we suggest is Walcott Tuff A. Note that all values are elemental percentages, not weighted for respective feldspar stoichiometric ratios.

10.34 ± 0.03 Ma (Table 4, corrected for a common standard). Our age analyses yield two distinct groupings of ages, one at 10.22 ± 0.01 and the other at 10.41 ± 0.01 Ma. By combining the Arbon Valley Tuff age determinations, in a similar manner to what *Kellogg et al.* [1994] and *Morgan and McIntosh* [2005] have done, yields a combined age of 10.27 ± 0.01 Ma. *Drew et al.* [2013] reported an age of 10.44 ± 0.27 Ma using U/Pb on the upper welded tuff horizon of two distinct horizons of the Arbon Valley Tuff, the lower of which they interpret as a poorly lithified surge deposit. However, as discussed below, we interpret these results to indicate the presence of two closely spaced eruptions, which we call Arbon Valley Tuff A and Arbon Valley Tuff B. We will discuss this interpretation in greater detail later in the text.

4.2. Paleomagnetic Analysis

The results from our paleomagnetic analysis for the Picabo and Heise volcanic fields are shown in Tables 5, 6, and Figure 4 and are divided between those volcanic units where unit means were determined and those where only site means are available. The main carrier of paleomagnetic remanence in the units studied is fine-grained single-domain magnetite [see *Anders et al*. 1989]. The presence of these carriers is seen in the response of individual samples to alternating field (Af) cleaning. In most samples the natural remanent (NRM) direction is within a few degrees of the site mean after Af cleaning at a minimum of 50 mT. Unlike the intermediate-polarity Huckleberry Ridge Tuff of the younger Yellowstone volcanic field [*Reynolds*, 1975], secondary magnetic minerals such as geothite are rare and site mean α_{95} values are small, typically less than 5°. The ashfall tuff that were examined (Table 5) proved to be more problematic with some samples showing wide swings in magnetic direction away from the well-grouped NRM directions as Af demagnetization increased in intensity [see *Anders*, 1990].

Results from the ignimbrites in the WO-2 core provide inclination values that are remarkably close to unit mean inclinations determined from ignimbrite outcrops on the margins of the eastern Snake River Plain (Table 6). The α_{95} values for the WO-2 samples were generally larger than those for the same units sampled from the margins of the eastern Snake River Plain. This is in part due to the limited number of samples from each contiguous section of core. The lowermost unit in the WO-2 core, the 6.66 Ma Blacktail Creek Tuff, has the same inclination of $I = 66.0°$ as the outcrop unit mean of $I = 66.5°$ [from *Anders et al*., 1993]. The mean inclination of the Walcott Tuff A in WO-2 of $I = 71.8°$ (Table 6) closely matches the inclination of the site mean of $I = 71.3°$ from a horizontal outcrop at American Falls. Higher in the WO-2 core Walcott Tuff B has an inclination of $I = 77.8°$ in WO-2 matches the outcrop-based unit mean inclination of $I = 77.4°$ [*Anders et al*., 1993] from along the northern margin of the eastern Snake River Plain. Still higher in WO-2, the Conant Creek Tuff yields an inclination of $-49.3°$ which compares well with the outcrop-based, tilt-corrected site mean of $-49.9°$ [*Reynolds*, 1975]. The uppermost ignimbrite in WO-2, which we interpret to be the tuff of Elkhorn Spring, has an inclination of $-43.9°$ which compares well with the tilt-corrected inclination value of $-46.4°$ from its lone surface outcrop at Heise Cliffs (Figure 2a).

Paleomagnetic study of the WO-2 core shows that there has been little or no tilting of units since acquisition of their stable remanent directions. This is true throughout the sequence, from the 6.66 Ma Blacktail Creek Tuff to the 5.52 Ma tuff of Elkhorn Spring. As we will discuss in detail below, we interpret the absence of tilting to indicate that none of ignimbrites sampled in the WO-2 core were involved in extensive caldera collapse deformation. Instead, the location of WO-2 (Figure 2b) is beyond the caldera boundaries as defined by *Pierce and Morgan* [1992] and *Morgan and McIntosh* [2005].

4.3. Feldspar Geochemical Analysis

Petrographic analysis of phenocryst populations of ignimbrites from the Picabo and Heise volcanic fields shows that sanidine and plagioclase are dominant with lesser quartz, minor amphibole, zircon, magnetite, and trace biotite. The relative concentration of nonglass minerals and fragments is variable depending on sampling site and degree of welding.

Results from our microprobe analyses of individual feldspar grains are shown in Figure 5 and in Table S1 (supporting information). Crystals do not exhibit significant chemical zonation from rim to center, so mean compositions for each sweep are shown. Of the nine major element concentrations determined for each sample, Na_2O, CaO, and K_2O best discriminate the tuff units (Figure 5). Figure 5a represents all feldspar analyses from this study. Solid circles represent samples from outcrops along the margins of the eastern Snake River Plain, while open symbols represent samples taken from the WO-2 core. In general, there is a significant overlap of compositions for both sanidine and plagioclase.

Figure 5b plots the averaged values of all measurements from outcrops of the various ignimbrite units including averaged microprobe-determined values from *Henshaw* [2002] (crosses in Figure 5b). Also shown is the averaged value from the tuff at a depth of 3760.8 in WO-2, which we previously correlated to the tuff of Elkhorn Spring. In Figure 5b the greatest separation in sanidine chemistry is between the WO-2 3760.8 sample and the Kilgore Tuff sample. Therefore, the paleomagnetism, $^{40}Ar/^{39}Ar$, and sanidine chemistry results are consistent with WO-2 3760.8 correlating with the tuff of Elkhorn. We recognize that the similarity of paleomagnetic orientations between the two units, the large errors in the age determination, and the

relatively tight grouping in feldspar chemistry leaves some room for interpretation involving this proposed correlation which we will discuss later in the text. Given these limitations, it is our interpretation that there is no Kilgore Tuff found in the WO-2 core.

Feldspar chemistry data from all outcrops of the Blacktail Creek Tuff, including those reported by *Henshaw* [2002], define a very tight grouping (Figures 5a and 5b). When we first examined the WO-2 core, we thought there was an apparent discontinuity at WO-2 4955 (Figure 3) separating two units with remarkably similar physical characteristics. However, feldspars from WO-2 4940.1 and WO-2 4998.8 have overlapping compositions despite the fact that these core samples are nearly 18 m apart. Based on the similarity of results from geochemistry, geochronology, and paleomagnetism, we interpret that both core samples are from a single eruption of the Blacktail Creek Tuff and that the apparent discontinuity may simply be a compound cooling of the same eruption.

Another stratigraphic problem is whether the Walcott Tuff B and the Walcott Tuff A are the same eruption, as suggested by *Morgan and McIntosh* [2005]. Figure 5c shows plagioclase and sanidine geochemistry of the Walcott Tuff. Solid circles are the averaged values from outcrops of either the Walcott Tuff B or the Walcott Tuff A. The solid cross is the averaged values of the Walcott Tuff B from *Henshaw* [2002]. The open circles are averaged analyses of samples from a common depth in the WO-2 core with the open blue circles from WO-2 4237.0 and green from WO-2 4250.4. In other words, green represents our preferred interpretation of Walcott Tuff A and blue our preferred interpretation of Walcott Tuff B. The plagioclase values do not discriminate between the tuffs, but there is a distinct, though minor, separation of sanidine values between Walcott Tuff A and Walcott Tuff B. Although the separation is not substantial, it is distinct. Further discussion of the Walcott A and B separation is presented below.

5. Discussion

5.1. Heise Volcanic Field and WO-2 Stratigraphy

The WO-2 borehole recovered over a 1.5 km nearly continuous core including more than a kilometer of eastern Snake River Plain basalts and most of the major ignimbrites emanating from the Heise volcanic field (Figure 3). At the bottom of the core is the oldest of the Heise volcanic field eruptions, the 6.66 Ma Blacktail Creek Tuff with six younger ignimbrites above it including the youngest, the 5.52 Ma tuff of Elkhorn Spring. The only major Heise volcanic field ignimbrite missing is the youngest unit, the 4.61 Ma Kilgore Tuff. The age, thickness, texture, and sequence of these units provide insight into their lateral extent, number of eruptions, and caldera locations. Based on our assessment of the $^{40}Ar/^{39}Ar$ dating, paleomagnetism, petrography, and feldspar chemistry data, there are several results that seem inconsistent with interpretations based on surface exposures. These interpretations include identification of a small early eruption of the Walcott Tuff and the proposed correlation between the Conant Creek Tuff and the tuff of Elkhorn Spring.

5.1.1. Walcott Tuff A and B

Directly above the rhyolite of Lower WO-2 is an ignimbrite we identified as the 6.26 ± 0.02 Ma Walcott Tuff A (Figure 3). The Walcott Tuff B sampled at American Falls yields an age of 6.27 ± 0.01 Ma—essentially the same age. Elsewhere, the Walcott Tuff was dated using K/Ar at 6.26 Ma by *Marvin et al*. [1970] (corrected for new decay constants) [*Dalrymple*, 1979] and using K/Ar at 6.36 Ma (corrected for decay constants) by *Armstrong et al*. [1975] with no distinction between Walcott Tuff A and Walcott Tuff B. Morgan and McIntosh dated this unit at 6.30 ± 0.05 Ma using $^{40}Ar/^{39}Ar$ (Table 4; assumes a 2 σ error and corrected for a common monitor standard) and again with no distinction between A and B eruptions. Along the northern margin of the eastern Snake River Plain we dated what was previously described as the tuff of Blue Creek [*Embree et al*., 1982] at 6.27 ± 0.01 Ma (Table 1) and what we are now calling Walcott B. The Walcott Tuff as described in the American Falls area [*Stearns and Isotoff*, 1956] and the tuff of Blue Creek [*Embree et al*., 1982] along the northern margin were proposed to be the same unit by *Morgan and McIntosh* [2005] and *Pierce and Morgan* [2009]. Given their nearly identical $^{40}Ar/^{39}Ar$ ages, it seems reasonable to assume they are products of the same eruption. However, a correlation of Walcott Tuff B between north and south of the eastern Snake River Plain is supported by the remarkable similar section at Howe Point [*Morgan and McIntosh*, 2005, Appendix 1] and that found near American Falls [*Carr and Trimble*, 1963]. *Carr and Trimble* [1963] report that the Walcott Tuff is as much as ~15 m thick and divided into two members. The upper member is a welded ignimbrite with a

brick-red vitrophyre near its top grading down to a densely welded black vitrophyre and a lower member that is a ~ 3 m of ashfall material. The Walcott Tuff at Howe Point is described as a ~55 m thick ignimbrite with a distinctive thick brick-red vitrophyre near its top and a dense black vitrophyre at its base which overlies ~3.5 m thick ashfall tuff [*Hackett and Morgan*, 1988, p. 298; *Morgan and McIntosh*, 2005, Appendix 1]. In WO-2 there is a stratigraphic sequence that is similar to those at American Falls and Howe Point that includes an upper 26.8 m thickness of ignimbrite with similar characteristics to the ~55 m section at Howe Point including the brick-red colored vitrophyre toward its top and a densely welded black vitrophyre overlying 3 m of ashfall at its base.

Below the ashfall at Howe Point is a ~1 m thick ignimbrite which is a tan-orange color and poorly welded [*Hackett and Morgan*, 1988; *Morgan and McIntosh*, 2005, Appendix 1]. In WO-2 the unit directly below the ashfall layer is a 3.5 m thick ignimbrite that has a densely welded black vitrophyre that grades downward to a gray poorly welded ignimbrite. Thin section examination of the upper vitrophyre reveals the majority of glass shards are orange in color. Both the ignimbrites are crystal poor with plagioclase the dominant feldspar which is similar to what we found for the ignimbrite overlying the ashfall at Howe Point and in WO-2 that we are calling Walcott Tuff B.

It is our contention that the ignimbrite found below the ashfall is a cycle eruption of the Walcott Tuff we are calling Walcott A. The age of Walcott A is the same as Walcott B within measurement precision (Tables 1 and 3), the paleomagnetic inclination between Walcott A and B in WO-2 and the unit mean direction are within a few degrees (Tables 5 and 6), and the plagioclase chemistry overlaps (Figure 5a). There are some differences: the paleomagnetic inclinations are slightly different between A and B within WO-2 (Table 6) and the sanidine chemistry (Figure 5c) exhibits slightly different domains. Overall, these similarities are suggestive of a common magma source. Walcott Tuff A and B exhibit an eruption pattern similar to the Yellowstone volcanic field eruptions where there are three cycle eruptions of the Huckleberry Ridge Tuff and the two associated with the Lava Creek Tuff with only slight differences in age, paleomagnetism, and chemistry [*Reynolds*, 1975; *Christiansen*, 2001; *Ellis et al*., 2012].

There is no discernable ignimbrite under the ashfall member of the Walcott Tuff B as described by *Carr and Trimble* [1963] at American Falls. However, they describe the uppermost Neeley Formation at the contact with the ashfall member as "Tan to orange, tuffaceous clayey sandstone, and tuff" [*Carr and Trimble*, 1963, p. G15]. We suggest the upper Neeley Formation tuff is possibly a distal extent of Walcott A seen at Howe Point as an "ignimbrite, dark yellowish orange" [*Morgan and McIntosh*, 2005, Appendix 1].

5.1.2. Conant Creek Tuff and Tuff of Elkhorn Spring Correlation

The Conant Creek Tuff was first described by *Christiansen and Love* [1978] based on exposures along the western flank of the Teton Range. *Love et al*. [1992] mapped the unit at Signal Mountain in Jackson Hole, Wyoming. *Gilbert et al*. [1983] further identified it in core from under the Jackson Lake Dam. The tuff of Elkhorn Spring was described by *Prostka and Embree* [1978] as forming a prominent part of the Heise Cliffs of Swan Valley, Idaho (Figure 2). It was suggested by *Morgan* [1992, p. 224] that the Conant Creek Tuff "may actually consist of two separate ignimbrites: (1) an older unit that is tentatively correlated with the tuff of Elkhorn Spring and (2) a younger unit that is correlative with the Kilgore Tuff". *Morgan and McIntosh* [2005] date the tuff of Elkhorn Spring from the Heise Cliffs in Swan Valley at 5.55 ± 0.13 Ma (error 2 σ and corrected for a common standard) and the Conant Creek Tuff on the west flank of the Teton Range (Hominy Ridge) at 5.70 ± 0.19 Ma (by step heating, corrected for a common standard, see appendix in *Morgan and McIntosh* [2005]), then reported mean age of 5.55 ± 0.13 Ma for the Conant Creek Tuff (Table 4; all ages corrected for common monitor standard age). As explained below, our results suggest the correlation between the Conant Creek Tuff and the tuff of Elkhorn Spring is not correct.

We determined an age of 5.52 ± 0.03 Ma (error 1 σ, Table 4) for the tuff of Elkhorn Spring at Heise Cliffs, which is within statistical variance of the 5.55 ± 0.13 Ma (error 2 σ, and corrected for a common standard) age in *Morgan and McIntosh* [2005] at the same location. Note that *Anders et al*. [2009, Figure 1] erroneously list the tuff of Elkhorn Spring as 4.46 Ma but in the text refer to it as 5.46 Ma; based on a 28.02 Ma Fish Canyon Tuff standard. As stated previously, the uppermost ignimbrite unit in WO-2 yielded an age of 5.45 ± 0.05 Ma (Table 3), and we correlated it to the tuff of Elkhorn Springs.

Love et al. [1992] mapped two ignimbrites at Signal Mountain—the 2.13 Ma Huckleberry Ridge Tuff and the Conant Creek Tuff. However, *Morgan and McIntosh* [2005] suggested that *Love et al*. [1992] and *Gilbert et al*. [1983] incorrectly identified the Conant Creek Tuff at Signal Mountain. They suggested this unit is instead the

Kilgore Tuff, and they report a date of 4.58 ± 0.07 Ma (error 2 σ, and corrected to a common age 28.201 Ma Fish Canyon Tuff standard). J. David Love and Claude M. Fountain sampled what is mapped as Conant Creek Tuff at Signal Mountain for the express purpose of $^{40}Ar/^{39}Ar$ dating at Lamont-Doherty Earth Observatory AGES laboratory. Using these samples, we date the middle and lower unit mapped by *Love et al.* [1992] and found the lower unit TCC (Table 1) yields an age of 6.01 ± 0.07 Ma and the middle unit SMK (Table 1) as 4.58 ± 0.07 Ma. Clearly, *Morgan* [1992] was correct in that the Conant Creek Tuff (as mapped by *Christiansen and Love* [1978]) is actually two units, the upper being the Kilgore Tuff. However, it is our opinion that the lower unit is not correlated to the tuff of Elkhorn Springs and is older with an age of 6.01 ± 0.07 Ma. *Christiansen and Love* [1978] dated the lowest stratigraphic horizon of the Conant Creek Tuff on the west flank of the Teton Range using K/Ar and got an age of 5.99 ± 0.08 Ma (when corrected for the *Min et al.* [2000] decay constant [*Dalrymple*, 1979]).

The confusion in unit identification is compounded by the report in *Morgan* [1988, p. 54] of the Conant Creek Tuff at Signal Mountain having a normal polarity ($I = 66.3°$, $D = 144.7°$) when both the Kilgore Tuff and Conant Creek Tuff clearly have a reversed polarity [e.g., *Reynolds*, 1975; *Anders et al.*, 1989; *Anders et al.*, 1993; *Morgan and McIntosh*, 2005]. Moreover, *Morgan and McIntosh* [2005] do not report Conant Creek Tuff on Signal Mountain when our results show the Conant Creek Tuff at the base of the outcrop mapped by *Love et al.* [1992]. This suggests to us that the original "type sections" of the Conant Creek Tuff on the west flank of the Teton Range is also comprised of two units, the Kilgore Tuff overlying the Conant Creek Tuff. Our age of 6.01 ± 0.07 Ma for the Conant Creek Tuff at Signal Mountain is further supported by $^{40}Ar/^{39}Ar$ dating of a unit in WO-2 that yields an age of 6.01 ± 0.01 (Table 3, WO-2 3802). No other Heise volcanic field unit we know of has a ~6 Ma age providing support to our interpretation that the Conant Creek Tuff is present in WO-2 and on Signal Mountain.

We conclude that the tuff of Elkhorn Spring and Conant Creek Tuff are separate units. The tuff of Elkhorn Spring is presently only found in outcrop at the Heise Cliffs in Swan Valley and in the WO-2 borehole. However, the similarity in chemistry [*Morgan*, 1992], petrography, and age suggest the Conant Creek Tuff and tuff of Elkhorn Spring may well represent eruptive events from the same, or nearly the same, caldera.

5.2. Picabo Volcanic Field

The Picabo volcanic field is poorly defined in both time and space. As we define it here, eruptions in the volcanic field initiated with the first eruption of the Arbon Valley Tuff and ended with the volumetrically smaller tuff of American Falls defined by a single proximal ignimbrite outcrop northeast of American Falls (Figure 2). A boundary for the Picabo volcanic field is shown in *Pierce and Morgan* [1992] and in *Drew et al.* [2013], but it is unclear how these boundaries are defined. Here we define the Picabo volcanic field in time and space as (1) including those units whose source is found between the location of the Twin Falls volcanic field [*Bonnichsen et al.*, 2008] and the caldera we define for the Blacktail Creek Tuff (Figure 2) and (2) having ages between 10.41 Ma and 6.66 Ma. As we discuss below, there are problems with this simple approach. However, for the purposes of assessing the migration rate of the Yellowstone-Snake River Plain volcanic system we are using the areal distribution of the Arbon Valley Tuff as a proxy for the position of the hotspot at 10.27 Ma.

5.2.1. Picabo Volcanic Field Versus Twin Falls Volcanic Field

The Yellowstone volcanic field and Heise volcanic field have no overlap in ignimbrite ages as there is between the Picabo and Twin Falls volcanic fields. If, as presented in *Pierce and Morgan* [1992, 2009] and in *Perkins and Nash* [2002], the age of the Twin Falls volcanic field ranges from 10.5 to 8.6 Ma and the age of ignimbrites emanating from the Picabo volcanic field are between 10.41 Ma and 7.58 Ma, then there is a potential problem in assigning particular outcrops to respective volcanic fields based on age alone. Critical to this problem are ignimbrites located between longitude 112.5° and 114° west (Figure 2). The units along the northern margin of the eastern Snake River Plain that fall within this spatial and temporal range are the tuff of Kyle Canyon, tuff of the Lost River Sinks, tuff of Appendicitis Hill, and tuff of Little Chokecherry Canyon. Also, *Michalek* [2009] identified three other ignimbrites in the Lake Hills area: Idavada "older" (Tivo) dated at 9.16 ± 0.20 Ma and 9.21 ± 0.18 Ma, (corrected for a common standard to 9.22 ± 0.20 Ma and 9.27 ± 0.18 Ma), Idavada "middle" (Tivm) dated at 8.39 ± 0.54 Ma (corrected to 8.44 ± 0.54 Ma), and Idavada "younger" (Tivy) dated at 8.76 ± 0.38 Ma (corrected to 8.82 ± 0.38 Ma). *Michalek* [2009] suggested Tivo correlated with the tuff of Appendicitis Hill and Tivy and Tivm correlated with the tuff of McMullen exposed on the southern margin of the eastern Snake River Plain, both of which are interpreted to be associated with the Twin Falls volcanic

field [see *Perkins and Nash*, 2002]. Alternatively, based on age dating alone, these units could be equivalent to the 9.28 ± 0.01 Ma tuff of Kyle Canyon and 8.87 ± 0.16 Ma tuff of the Lost River Sinks found at Howe Point, both closer to the source of the Picabo volcanic field than the Twin Falls volcanic field. The petrography of the tuff of Kyle Canyon and Tivo are similar, with similar phenocryst ratios of amphibolite to plagioclase to magnetite/ilmenite [*Michalek*, 2009]. In outcrop there are two tuffs associated with the tuff of Kyle Canyon at Howe Point. The upper ignimbrite is ~50 m, and the lower ashfall tuff ~1 m [*McBroome*, 1981]. Tivo is also composed of two units in the Lake Hills; the thicker flow is ~60 m, and the thinner is ~40 m [*Michalek*, 2009].

The Picabo Tuff [*Garwood et al*., 2011] is located near the town of Picabo, Idaho, (Figure 2) and was dated by K/Ar at 8.98 ± 0.12 Ma [*Honjo et al*., 1986]. The tuff is geographically closer to the Twin Falls volcanic field or the Magic Reservoir volcanic center of *Leeman* [1982b] than to the Picabo volcanic field (Figure 1) and, as discussed in *Leeman* [1982b], *Schmidt* [1961, 1962] reports that the Picabo Tuff increases in welding toward the Magic Reservoir (Figure 2) rather than toward the Picabo volcanic field. This would make the Picabo Tuff an unlikely candidate for emanating from the Picabo volcanic field.

Given the name Picabo for both the Picabo Tuff and the Picabo volcanic field [*Pierce and Morgan*, 1992], we suggest that in the future what is called the Picabo volcanic field might be better represented as the Arbon Valley volcanic field, named after the most extensive of ignimbrite attributed to it. A list of the silicic volcanic units we suggest are included in the Picabo volcanic field are in Table S2. Further work is needed in order to make clear distinctions between products of the Picabo volcanic field (Arbon Valley volcanic field?) and that of the Twin Falls volcanic field (Figure 1) as there is clear overlap in time and space between units from these two volcanic fields.

5.2.2. Arbon Valley Tuff A and B

There is a significant range of ages reported for the Arbon Valley Tuff Member of the Starlight Formation (called the Arbon Valley Tuff or Arbon Valley Tuff A and B in our results, Table 2) reported by *Kellogg et al*. [1994], *Morgan and McIntosh* [2005], and *Drew et al*. [2013]. In most places where we sampled the Arbon Valley Tuff it is poorly welded or an ashfall; however, we sampled a densely welded ignimbrite southwest of Fort Hall (Figure 2a). Though we did not observe two distinct eruptive events within the outcrops at Fort Hall, we previously described an ashfall tuff equivalent (VPT-1 of *Anders et al*., 2009) in Grand Valley, Idaho, that exhibited distinct depositional and mineralogical boundaries. *Trimble* [1976] described two ignimbrite cooling units associated with the Arbon Valley Tuff at a location ~10 km east of American Falls (Figure 2). At some localities there are two cooling units, while at others there is only a single cooling unit [*Trimble*, 1976; *Kellogg et al*., 1994]. [*Drew et al*., 2013, Appendix 2] observed two distinct horizons but observed no cooling breaks. They interpreted the lower horizon to be a surge deposit. Although we did not sample these two layers at a single location, our $^{40}Ar/^{39}Ar$ analyses of this unit showed two distinct populations. Based on these results, we suggest there were two eruptions, one at 10.41 ± 0.01 Ma recorded by the Arbon Valley Tuff A and one at 10.22 ± 0.01 Ma recorded by the Arbon Valley Tuff B. Argon-40/Argon-39 samples collected from individual sites showed a mixture of ages that we interpreted to indication inclusion of older material in the youngest eruption. This assumes there is not a systematic radiogenic argon loss or ^{36}Ar excess within feldspars from a single eruption. If the age groupings are from the same eruption as suggested by *Morgan and McIntosh* [2005], our combined age is 10.27 ± 0.01 Ma compared to 10.34 ± 0.03 Ma (corrected to a common standard) of *Morgan and McIntosh* [2005] in Table 4 and 10.25 Ma (corrected to standard MMhb-1 of *Renne et al*. [1998] from *Kellogg et al*. [1994].

An older U/Pb zircon age of 10.44 ± 0.27 Ma from the upper horizon of the Arbon Valley Tuff is reported by *Drew et al*. [2013]. We suggest that because the age determination was from the core of individual zircon grains in their study, the resulting U/Pb age represents an early formed grain in the pre-eruption melt. Similarly, the other sites where we dated a unit using $^{40}Ar/^{39}Ar$ on feldspars, Drew et al. got a slightly older age—the exception being the tuff of Lost River Sinks where their age is much younger (Table 4).

5.3. Heise Volcanic Field Calderas

The calderas of the Heise and Picabo volcanic fields are buried under more than 700 m of basalt and sediment that have filled in the eastern Snake River Plain downwarp [*Rodgers et al*., 2002]. One of the few ways to assess the position of these long-since inactive calderas is through geophysical techniques like seismic refraction and reflection imaging or resistivity studies, though none are particularly useful in defining a caldera's location through hundreds of meters of basalt flows. However, the advent of drilling through basalt and into rhyolitic

rocks at the Idaho National Laboratory site has proved extremely valuable. These include boreholes 2-2A, INEL-1, and WO-2. Here we have used the data from WO-2 combined with data from other boreholes and the volcanic rocks along the margin of the eastern Snake River Plain to help further define the boundaries of calderas. Relocating these caldera locations can be used to test whether their locations are consistent with an independent estimate of North American plate migration rate—as we would predict for a fixed hotspot source.

5.3.1. Blacktail Creek Tuff Caldera

The location of the caldera of the Blacktail Creek Tuff is critical to assessing migration rates as it is the first eruption of the Heise volcanic field and the largest [cf. *Morgan and McIntosh*, 2005]. Gravity data [e.g., *Mabey et al*., 1974] provide little or no help in identifying the caldera's location since the thickness variation of basalts and sediment interbeds are mostly unknown. Two deep-drilling boreholes provide the most significant information on the subsurface. These are the 1.5 km WO-2 borehole and the 3 km INEL-1 borehole (Figures 1 and 2). Only sporadic core was recovered from INEL-1, but continuous core with excellent preservation was recovered from WO-2. In the WO-2 recovered core we identified two thick rhyolite lavas, the rhyolite of Upper WO-2 and the rhyolite of Lower WO-2. The lower rhyolite lava is over 200 m thick, is ~0.2 m.y. younger than the Blacktail Creek Tuff, and possibly represents several individual lavas. One interpretation of the thick rhyolite of Lower WO-2 is that it is an intracaldera lava restricted to infilling of the caldera collapse. Another interpretation is that it is overflow of intracaldera lavas, similar to the post-Lava Creek Tuff rhyolite lavas found in Yellowstone that extend as much as 25 km from its caldera boundaries [*Christiansen*, 2001]. The paleomagnetically determined inclination of the Blacktail Creek Tuff in WO-2 is identical to the inclination of the mean site in untilted outcrops (Tables 5 and 6), which indicates little or no tilting since deposition. We suggest that if WO-2 had drilled into a caldera, then the Blacktail Creek Tuff should exhibit significant tilting due to posteruptive caldera collapse and doming. One possible explanation of the lack of tilt is that the Blacktail Creek Tuff in WO-2 is intracaldera ignimbrite fill. An ignimbrite infill might acquire its Thermal Remnant Magnetization (TRM) after caldera collapse was completed; thus, the TRM would not have been affected by the collapse. However, missing in WO-2 are some of the features that might be expected of caldera collapse infill in a location near a caldera margin (Figure 2b). These include slide breccias composed of younger rocks, conglomerates eroded from the rims, and lake sediments [*Lipman*, 1997]. There is no evidence of these kinds of deposits between the bottom of WO-2 and the base of the Walcott Tuff A (Figure 3). Moreover, if WO-2 was located within a collapsed caldera, we would expected that the rhyolite of Lower WO-2 would be associated with doming in the caldera floor causing deformation of the underlying Blacktail Creek Tuff. An anomalously thick section of the Blacktail Creek Tuff in WO-2 could also be evidence of proximity to its caldera source, but this evidence is lacking since WO-2 core terminates after passing through 18 m of section. Except for a few centimeter-scale pumice fragments and some feldspar grains up to 5 mm, there is no textural evidence that the Blacktail Creek Tuff in WO-2 is a proximal deposit.

From all of the above we conclude that the Blacktail Creek Tuff caldera is located further to the east-northeast from WO-2 than previously interpreted. How far to the northeast depends on the same criteria used in previous studies of the distribution and thickness of the tuff [e.g., *Embree et al*., 1982; *Morgan et al*., 1984; *Pierce and Morgan*, 1992; *Morgan and McIntosh*, 2005]. The thickest surficial deposits of the Blacktail Creek Tuff found on the margins of the Snake River Plain are located the farthest to the northeast (Figure 2b) in the Big Hole Mountains (150 m thick) south of the Snake River Plain and in the southern Beaverhead Mountains (100 m thick) [*Skipp*, 1984] north of the Snake River Plain. Younger eruptive events to the northeast likely explain why there is no gradual reduction in thickness to the northeast of these thick outcrops. This distribution pattern suggests that the caldera for the Blacktail Creek is farther to the northeast than estimated by *Pierce and Morgan* [1992] and *Morgan and McIntosh* [2005]. Furthermore, several ignimbrites previously thought to be the westernmost outcrops of the Blacktail Creek Tuff [*Anders et al*., 1993; *Snider*, 1995], east of Arco, Idaho, (Figure 2) are now known to be the older tuff of Kyle Canyon and tuff of Little Chokecherry Canyon of the Picabo volcanic field. Also, there is a present-day southwest topographic gradient, if such a gradient existed during the eruption of the Blacktail Creek Tuff, ignimbrite flow might extend disproportionally downhill to the southwest. This could be why the more recent Huckleberry Ridge Tuff B is found farther from its source to the southwest than any other direction. In conclusion, although WO-2 is located within or at the edge of the Blacktail Creek Tuff caldera in *Pierce and Morgan* [1992] and *Morgan and McIntosh* [2005], we reinterpret the location of the caldera farther to the east-northeast (see Figures 1 and 2b). Based on our interpretation of the distribution of thicknesses (Figure 2b) and proximal facies, we shift center of the Blacktail Creek Tuff caldera to the northeast so that it is now 118 km southwest of the center of the Huckleberry Ridge Tuff caldera (Figure 2b) as defined by *Christiansen* [2001].

We estimate a volume of ignimbrite at roughly 1500 km^3 for the Blacktail Creek Tuff by assuming an elliptical cone with height of 200 m and using our distribution of ignimbrite deposits (Figure 2b). The 200 m height value was based on back calculating for height from the estimate of volume and areal extent of the better exposed Kilgore Tuff as presented in *Morgan and McIntosh* [2005]. Our estimate of ignimbrite from the Blacktail Creek Tuff eruption is greater than their 1200 km^3 estimate even considering that we believe they reported ignimbrite farther north and west than outcrops justify. For comparison *Christiansen* [2001] estimates an area of 15,400 km^2 and a volume of 1340 km^3 for the Huckleberry Ridge Tuff B, which yields a height of 261 m, again assuming an elliptical conical distributed volume. If we use a height estimate of 261 m for the Blacktail Creek Tuff, we get a volume of 1980 km^3. All these estimates assume a conical or elliptical cone shape for which there is little or no evidence that such a volume distribution exists and the central regions are not known. Moreover, our estimate of ignimbrite extent is a minimum as erosion and subsequent burial results in restrictive areal distribution, and our estimates do not include ashfall deposits.

5.3.2. Walcott Tuff A and B Calderas

Similar to lavas that overlie the Blacktail Creek Tuff in WO-2, there is a thick (95 m) rhyolite lava (6.21 ± 0.02 Ma rhyolite of Upper WO-2) or series of lavas that overlies Walcott Tuff B that might be expected of a posteruptive intracaldera rhyolite lava that is restricted to the caldera itself. However, as is the case with deposits overlying the Blacktail Creek Tuff, there is no evidence of breccia slides, conglomerates, or lake sediments in WO-2 between the Walcott Tuff B and the rhyolite of Upper WO-2 (Figure 3) as expected within the collapse depression [*Lipman*, 1997]. Moreover, the observation that the underlying Blacktail Creek Tuff in WO-2 is untilted supports the interpretation that the overlying Walcott Tuff A and B were not deformed as a result of either collapse or postcollapse dome formation or that the TRM was set after deformation.

It is clear that the limited thickness and poorly welded character of Walcott Tuff A at Howe Point, as well in WO-2, implies that its caldera source is to the east or southeast of these sampling sites. We are aware of no ignimbrite associated with the Walcott Tuff A that has been identified along the southern margin of the eastern Snake River Plain. However, if as we suspect, the upper Neeley Formation contains poorly welded to tuffaceous Walcott Tuff A; the implication is that the source is farther to the northeast from the American Falls area than the source of Walcott Tuff B. Previously, the position of the Walcott Tuff B caldera (often called the tuff of Blue Creek caldera) was based on seismic reflection and gravity data [*Mabey et al*. 1974; *Pankratz and Ackermann*, 1982]. In our view these data are insufficient to distinguish between our interpretation of the caldera's location and previous interpretations of the caldera's location [*Embree et al*., 1982; *Morgan et al*., 1984; *Pierce and Morgan*, 1992; *Morgan and McIntosh*, 2005]. Moreover, faulting at Howe Point thought to be related to caldera collapse rings [*Hackett and Morgan*, 1988] may well be unrelated to caldera collapse as the concordance of paleomagnetic inclinations of the Blacktail Creek Tuff within WO-2 and its unit mean direction on the margins of the eastern Snake River Plain suggest that overlying units were not tilted during a caldera collapse [*Anders et al*., 1993]. It is our interpretation that these faults are similar to those surrounding the eastern Snake River Plain and related to subsidence of eastern Snake River Plain due to volcanic loading [*Anders and Sleep*, 1992; *Rodgers et al*., 2002].

5.3.3. Kilgore Tuff Caldera

We found no evidence of the Kilgore Tuff in the WO-2 core and no mappable outcrops in the southern Lemhi Range [e.g., *Kuntz et al*., 2003] suggesting a limited westward spread of ignimbrite associated with this eruption. The Kilgore Tuff in INEL-1 core was reported by *McBroome* [1981]. A fission-track age of 4.2 ± 0.3 on the uppermost unit in INEL-1 [*Morgan et al*., 1984] is roughly consistent with the Kilgore Tuff. However, units deeper in the core, described as the tuff of Blue Creek and tuff of Edie Ranch [*McBroome*, 1981], were dated by U/Pb at over 8 Ma [*McCurry and Rodgers*, 2009]. That there is no mappable Kilgore Tuff at Howe Point [*Kuntz et al*., 2003, Figure 2] and the youngest ignimbrite at that location was also dated at 4.1 ± 0.6 Ma by fission track in the same study [*Morgan et al*., 1984] suggest that the INEL-1 Kilgore Tuff interpretation may also be erroneous. However, assuming the Kilgore Tuff was indeed found in INEL-1 and borehole 2-2A on the INEL site, these would represent the western limit of the Kilgore Tuff. The ignimbrite Kilgore Tuff on Signal Mountain (Figure 2) would represent the eastern limit. Therefore, this reduces the areal extent of Kilgore Tuff ignimbrite and consequently the volume of the Kilgore Tuff ignimbrites from *Morgan and McIntosh*'s [2005] estimate of 1800 km^3. *Morgan et al*. [1984] estimated 800 km^3 for the same eruption, so clearly, there is some flux in these estimates. We estimate a volume of ignimbrite at roughly 1100 km^3 for the Kilgore Tuff by assuming an elliptical cone where $h = 200$ m using

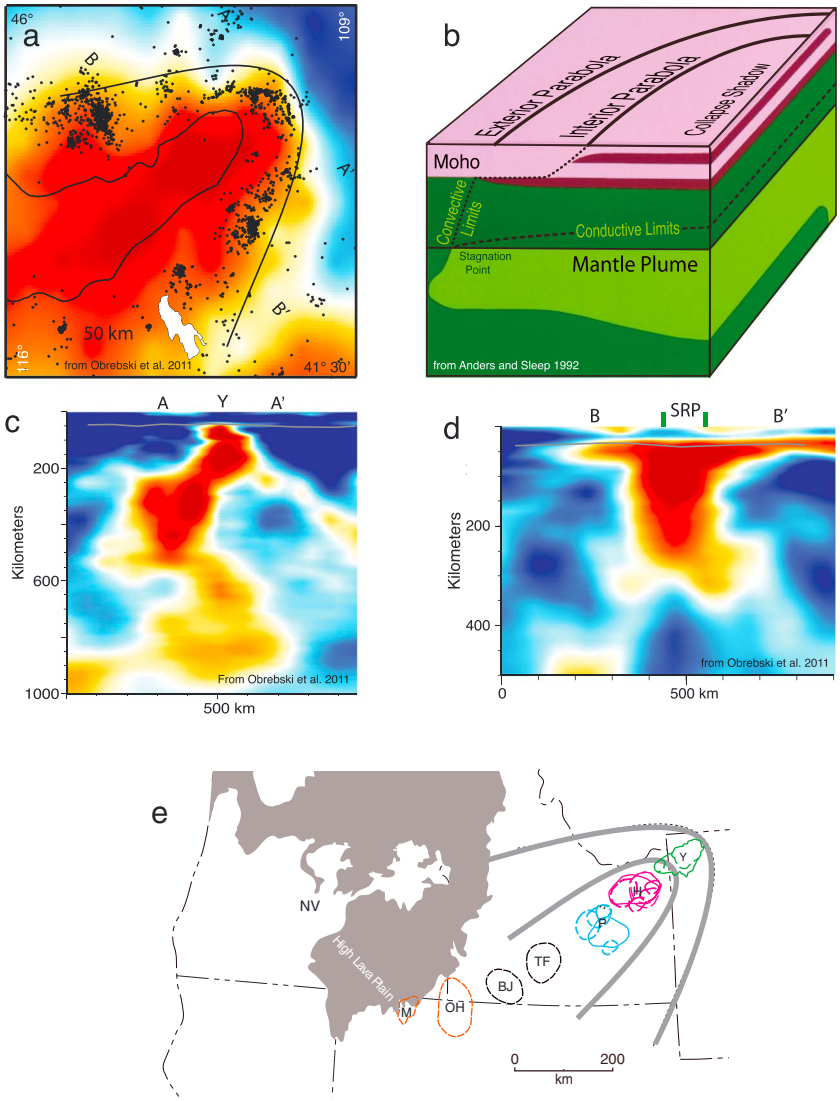

Figure 6. (a) Body wave velocity map at 50 km depth for the area surrounding the eastern Snake River Plain [from *Obrebski et al.*, 2011]. Lower velocities are in red, higher are in blue. Black dots are earthquakes and the parabola is from Figure 1. (b) Block diagram of the crust and upper mantle under the seismic parabolas of the northeast Basin and Range. Pink is the crust, dark green is the mantle, and light green is the Yellowstone hotspot plume at the base of the lithosphere. Parabolic shape of the exterior parabola is due to magmas (in red) rising from the parabolic-shaped Yellowstone plume. The interior parabola is the result of strengthening of the area under the eastern Snake River Plain resulting from midcrustal basaltic intrusions. Diagram is from *Anders and Sleep* [1992]. (c) Velocity structure under Yellowstone along profile B-B′ from *Obrebski et al.* [2011, Figure a]. (d) Velocity structure across the eastern Snake River Plain in profile A-A′ in Figure 1a. The high-velocity blue here is thought to be a fragment of slab. The low-velocity conduit here is thought to be the plume deflected to the northwest by the slab fragment. (e) Map of the northwestern United States with calderas associated with the Yellowstone-Snake River Plain silicic volcanic track. The McDermitt (M) and Owyhee-Humboldt (OH) are from *Pierce and Morgan* [1992], the Bruneau-Jarbidge (BJ) and Twin Falls (TF) Volcanic centers are from *Bonnichsen et al.* [2008], the Yellowstone volcanic field (Y) is from *Christiansen* [2001], and the Heise (H) and Picabo (P) volcanic field is from this study. HLP is the High Lava Plain with the Newberry Volcano (NV) representing the most northwestern extent of the Newberry trend [e.g., *Jordan et al.*, 2004]. Dark areas represent the Columbia River and Steens flood basalts from *Camp and Ross* [2004].

the same criteria discussed previously. If we assume a 261 m height estimate, we get a volume of 1380 km^3 for the Kilgore Tuff. As we discussed previously, our estimates of ignimbrite extent are both minimums as erosion and subsequent burial results in restrictive areal distribution, and our estimates do not include ashfall deposits, and we assume a conical distribution.

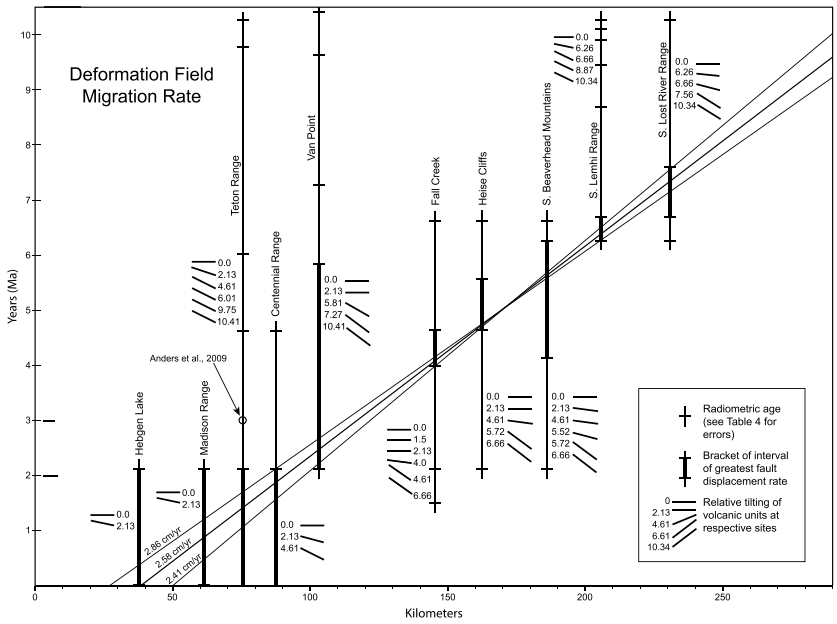

Figure 7. Plot of distance versus time for various normal faults. The locations are shown in Figures 1 and 2. Vertical lines represent the age span of the fault as defined by the volcanic rocks in the hanging walls and footwalls. Short horizontal lines intersecting the vertical line represent various volcanic units within the hanging walls and footwalls. Thick lines represent the temporal interval over which the greatest fault displacement occurred. Distance is measured between the respective hanging wall/footwall location and the parabola in Figure 1 along a line oriented N55°E. Short inclined lines with numbers assigned to each are the age and relative tectonic tilt of their respective hanging wall or footwall at each sampling site. The slope of the lines labeled 2.58 cm/yr represents the average of the possible velocities that fit each sampling site. The 2.58 cm/yr value is uncorrected for the 11% extension along the margin of the eastern Snake River Plain. Correcting that value yields a velocity of 2.38 cm/yr. For further details see *Anders et al.* [1989] and *Anders* [1994].

5.4. Picabo Volcanic Field Calderas

The only borehole that has implications to the location of Picabo volcanic field calderas is the INEL-1 where Picabo volcanic field rocks were encountered at depth of just below 1,000 m continuing down to the base of the borehole at 3,000 m [*McCurry and Rodgers*, 2009]. Of the Picabo volcanic field ignimbrites, the Arbon Valley Tuff caldera is the most useful for our study. As might be expected, as eruptions occur further back in time, it becomes more difficult to establish regional distribution which means it is more difficult to locate a source. Because of the unique chemistry and outcrop expression of the Arbon Valley Tuff, it is easily identified and its regional extent is the most easily established of the Picabo volcanic field ignimbrites.

5.4.1. Arbon Valley Tuff A and B Calderas

Based on a resistivity and gravity studies, *Kellogg et al.* [1994] place a caldera boundary they called the Tabor caldera as an arc with focus located about 15 km southwest of Blackfoot (Figure 2b). They also note that several rhyolite lavas a few hundred thousand years younger than the Arbon Valley Tuff, located along the southern margin of the Snake River Plain, help define the southern limits of the caldera. *Drew et al.* [2013] described some of these units described by *Kellogg et al.* [1994] as rhyolite lavas as ignimbrites. We generally agree with Kellogg et al. about the southern caldera rim boundary, but due to our identification of more extensive outcrops of the Arbon Valley Tuff on the northern margin of the Plain, we suggest the caldera is areally more extensive than indicated by *Kellogg et al.* [1994]. *Drew et al.* [2013] came to a similar conclusion in their placement of the Arbon Valley Tuff caldera (Figure 2b). Clearly, the greatest concentration of densely welded Arbon Valley Tuff ignimbrite is along the southern margin of the eastern Snake River Plain and centered around Fort Hall (Figure 2b). North of the Snake River Plain there are still substantial outcrop thickness in the Lost River and Lemhi Ranges, such as the Briggs Canyon and Lone Pine area (Figure 2). Therefore, we, as well as *Drew et al.* [2013], have extended the Arbon Valley Tuff caldera boundaries beyond what *Kellogg et al.* [1994] envisioned (Figure 2b).

5.4.2. Other Picabo Volcanic Field Calderas

U/Pb analysis of rhyolites from borehole INEL-1 yields ages between 8.04 Ma and 8.35 Ma placing them within the age span and geographic area of the Picabo volcanic field. *McCurry and Rodgers* [2009] described these older units as representing ~2.1 km thick of intracaldera volcanic facies although a distinction was not made between rhyolite lavas and ignimbrites (M. McCurry, personal communication, 2013). Given that these ages are slightly younger than the 8.87 Ma age of the tuff of the Lost River Sinks at Howe Point (Figure 2), it is reasonable to assume they are intracaldera lavas and ignimbrites. Therefore, this penetration by INEL-1 places the caldera source of the 8.87 Ma tuff of the Lost River Sinks (Table 4) along the northern margin of the eastern Snake River Plain. Since WO-2 is near borehole INEL-1 (Figure 2) and inboard of the Plain's margin, it too most likely overlies the caldera of the tuff of the Lost River Sinks.

Although the tuff of Kyle Canyon (Howe Point) and the older "Idavada" rhyolite (in an area ~10 km northeast of Picabo, Figure 2) have different thicknesses, both have similar outcrop expressions and petrography [*McBroome*, 1981; *Michalek*, 2009]. If these units are indeed from the same eruptions, this places the source farther away from Howe Point and closer to the Lake Hills where we have tentatively placed it (Figure 1). On the other hand, the tuff of Little Chokecherry Canyon and tuff of Appendicitis Hills are located at roughly equal distance from both the Heise and Twin Falls volcanic fields (Figure 1). We interpret that the tuff of American Falls (found in close proximity to the Picabo volcanic field), the tuff of Kyle Canyon, the tuff of the Lost River Sinks, and the tuff of Little Chokecherry Canyon as emanating from calderas in the Picabo volcanic field. Other volcanic units thought to be associated with the Picabo volcanic field are listed in Table S2 in the supporting information. Both our location of the Picabo volcanic field boundary and the boundary of the *Drew et al*. [2013] includes the INEL-1 borehole site, whereas the *Pierce and Morgan* [1992] does not. Our interpretation may stand to be corrected if later work identifies the rhyolites sampled by *McCurry and Rodgers* [2009] to be distal ignimbrites rather than intracaldera lavas. The selection of individual caldera locations for the Picabo volcanic field in Figure 1 is for the most part speculative and poorly constrained with the exception of the Arbon Valley Tuff. Clearly, more work is necessary on the correlation of units, and in locating the point of origin for lavas and ignimbrites younger than the Arbon Valley Tuff in the Picabo volcanic field.

5.5. Velocity of the North American Plate

Caldera locations in the Picabo and Heise volcanic fields provide important constraints on the progression of the North American Plate in a S55°W direction over the Yellowstone hotspot [e.g., *Pierce and Morgan*, 1992]. However, other techniques that calculate migration rates independent of caldera locations yield much slower rates [*Minster and Jordan*, 1978; *Gripp and Gordon*, 1990]. The difference is because caldera locations record not only the North American plate migration rate but also the extension rate internal to this region of North America—the northeastern Basin and Range Province.

The pattern of extension was addressed by *Anders et al*. [1989], *Pierce and Morgan* [1992], and *Smith and Braile* [1994], who demonstrated that seismicity and active normal faults in the northeastern Basin and Range are restricted to a parabolic zone (Figure 1) that migrates in tandem with the hotspot. *Anders and Sleep* [1992] and *Ribe and Christensen* [1994] suggested that the parabolic shape results from heat generated from a parabolic-shaped Yellowstone plume formed at the base of the lithosphere (Figures 6a and 6b). In other words, the interaction of the radial velocity field of the rising Yellowstone plume with North American plate linear velocity field results in the flow pattern at the top of the plume being formed into a parabolic shape. *Anders and Sleep* [1992] suggested the magma from partial melting of the top of the plume rises through the lithosphere. The result is that the crust that is already undergoing extension [see *Anders et al*., 2009] experiences increased heating at its base and concomitant accelerated extension near its surface. The distribution of heat from this process is represented by the parabolic shape to the region of low velocity imaged at a depth of 50 km by *Obrebski et al*. [2011] (Figure 6a). Moreover, *Kelbert et al*. [2012] using magnetotelluric data identified a 40 km to 80 km deep pattern of partial melt extending off the margins of eastern Snake River Plain that they suggested is coincident with the seismic parabola. *Anders and Sleep* [1992] and *DeNosaquo et al*. [2009] suggested the aseismic eastern Snake River Plain or collapse shadow (Figure 6b) is the result of lithospheric strengthening due to freezing of magmas intruded into the midcrustal levels [cf. *Parsons and Thompson*, 1991; *Parsons et al*., 1998; *Leeman et al*., 2008]. As *Anders and Sleep* [1992] suggested, the aseismic eastern Snake River Plain itself is moving southwestward as a coherent block thus making room for extension within the parabola—somewhat like pulling a slice out of a pizza pie and stretching the cheese along

its borders (Figure 1). This coherent block concept for the eastern Snake River Plain is supported by GPS campaigns and estimates of dike volume [*Chadwick et al*., 2007; *Holmes et al*., 2008; *Payne et al*., 2008, 2012] which demonstrate no measurable extension over decadal timescales and by estimates of Quaternary dike intrusions [*Holmes et al*, 2008] which yield extension rates and order of magnitude slower than the adjacent Basin and Range.

Thus, although the eastern Snake River Plain shows little evidence of active extension, this region was formerly extended when it passed over the hotspot and through the seismic parabola (Figures 1 and 6e). Whether extension occurred slightly northeast of, coincident with, or slightly southwest of the hotspot, the spacing of calderas on the eastern Snake River Plain records the combined rates of extension and plate migration since the caldera formed. Earlier workers did not take this into account so that migration estimates such as 2.9 cm/yr during the past 10 m.y. [*Pierce and Morgan*, 1992] are too fast. *Rodgers et al*. [1990, 2002] did account for this: using balanced cross sections along the southern Snake River Plain margin where they measured 15% to 20% extension cumulative extension, yielding extension rates of 0.4 to 0.6 cm/yr over 16 m.y. They subtracted this extension rate from Pierce and Morgan's caldera-based estimate of 2.9 cm/yr to derive a plate migration rate of 2.3 cm/yr to 2.5 cm/yr [*Rodgers et al*., 2002]. For this paper, we acknowledge that extension older than the Picabo and Heise calderas would not affect the spacing and use balanced cross sections with various timing constraints, as well as new mapping [*Rodgers et al*., 2006], to calculate 11% extension along the eastern Snake River Plain margins since ~10.3 Ma.

5.5.1. Plate Velocity Based on Caldera Locations

We now focus on the positions of the eastern Snake River Plain calderas through time to determine North American plate migration rates. Using *Pierce and Morgan*'s [1992] locations, we find the centers of the Picabo volcanic field and Huckleberry Ridge Tuff caldera (the first of the Yellowstone volcanic field eruptions) are 231 km apart. An age span of 8.14 m.y. between initial eruptions in these volcanic fields yields a migration rate of 2.84 cm/yr, which when corrected for 11% extension yields a migration rate of 2.56 cm/yr. Using our new location of the Arbon Valley Tuff (Figure 2b; first eruption of the Picabo volcanic field) caldera, we get a separation of 208 km, which using an 8.14 m.y. age span and 11% extension yields a corrected migration rate of 2.30 cm/yr. Similarly, using *Pierce and Morgan* [1992] caldera location for the Blacktail Creek Tuff (first eruption of the Heise volcanic field) and Huckleberry Ridge Tuff, we determine they are 133 km apart. An age span of 4.53 m.y. between eruptions yields a migration rate of 2.94 cm/yr, which when corrected for 11% extension becomes a migration rate of 2.65 cm/yr. Using our new location of the Blacktail Creek Tuff caldera (Figure 2b), we get a separation of 118 km, using a 4.53 m.y. age span and 11% extension yields a corrected migration rate of 2.35 cm/yr.

5.5.2. Plate Velocity Based on the Deformation Field

Anders et al. [1989] demonstrated that displacement along a major fault (the Grand Valley/Star Valley fault) was affected by the location of the Yellowstone hotspot. *Anders* [1994] showed that many of the faults within valleys surrounding the eastern Snake River Plain demonstrated a similar pattern and that the intervals of accelerated displacement rate defines the migration rate of the thermal effects of the hotspot. By plotting the timing of accelerated faulting against distance between faults in the direction of the hotspot track (S55°W), the velocity of the North American plate with respect to the Yellowstone hotspot can be assessed. The underlying assumption is that the thermal structure of the hotspot is symmetric about the axis of the hotspot track. Here we use this approach, described in more detail in *Anders* [1994], with two revisions to improve on the previous assessment of plate migration rate. First, we apply the new geochronology on the volcanic units as described above and second, we then apply the newly developed value of extension of 11% from *Rodgers et al*. [2006]. As can be seen in Figure 7, the best fit rate is 2.58 cm/yr averaged between the greatest and least velocity slope that fits all intervals of accelerated displacement. Adjusting the 2.58 cm/yr for 11% extension since 10.3 Ma yields a velocity of 2.38 ± 0.2 cm/yr which is slightly higher than the 2.2 ± 0.18 cm/yr from *Anders* [1994].

Overall, we use two independent techniques to calculate the velocity of the North American plate during the past 10 m.y. Analysis of the deformation field yields an extension-corrected rate of 2.38 ± 0.21 cm/yr. Analysis of the spacing of volcanic calderas yields an extension-corrected rate of 2.30 cm/yr for the interval between 10.27 Ma and 2.13 Ma and 2.35 cm/yr for the interval between 6.66 Ma and 2.13 Ma. These rates are close to the Yellowstone-independent rate determined by *Minster and Jordan* [1978] of 2.4 cm/yr *Gripp and Gordon* [1990] of 2.2 ± 0.2 cm/yr but lower than the 2.68 ± 0.78 cm/yr from *Gripp and Gordon* [2002]. It is therefore our

best estimate that the migration rate of silicic volcanism is constant and between 2.30 cm/yr and 2.38 cm/yr. A constant migration rates over the last 10 m.y. matches the prediction of what would be expected of a classical fixed deep-sourced hotspot. This does not exclude other interpretations but demands accounting in other proposed models.

5.6. Deep-Sourced Yellowstone HotSpot Model

Recent imaging has been used to suggest that the Yellowstone-Snake River Plain volcanic system is shallow sourced resulting from counterflow resulting from a sinking Juan de Fuca slab or slab fragments [*Faccenna et al*. 2010; *James et al*., 2011; *Fouch*, 2012]. There is a deflection in the pattern of the low-velocity conduit beneath Yellowstone-Snake River Plain track (Figure 6c) that *James et al*. [2011] suggest results in pressure-release melting in counterflow around the slab fragment, which they suggest is the source of the Yellowstone hotspot. However, there is a clear continuation of the low-velocity conduit down to ~900 km, and possibly to 1200 km, as seen in the model of *Obrebski et al*. [2010, 2011], well below the slab fragment (Figure 6c). There is no low-velocity conduit imaged below that depth. Nevertheless, its absence could be due to degrading resolution in the lower mantle (M. Obrebski, personal communication, 2013). Global models [e.g., *Montelli et al*., 2004] do not show any large-scale velocity conduit either below that depth. We also interpret the deflection of the low-velocity conduit as resulting from counterflow around the slab, but unlike *James et al*. [2011], we argue the sinking slab flows around a deep-sourced preexisting hotspot conduit or tail resulting in the observed deflection. As with any sinking object in a viscous medium, a counterflow will envelop the object by deflecting the flow lines around it (Figure 6c). Other evidence supporting a deep mantle source for the Yellowstone hotspot include (1) high $^{3}He/^{4}He$ ratios in excess of 15 (R/R_A) [*Graham et al*., 2009]. (2) Uplifting of the 660 km discontinuity by some 12 km to18 km directly below Yellowstone [*Schmandt et al*., 2012]. (3) *James et al*. [2011] argue that the edge effect of the slab fragment is consistent with the continued nature of the volcanism along the hotspot track; however, the vast bulk of midcrustal and near-surface basaltic volcanism is in place within 100 km southeast of Yellowstone [*Brott et al*., 1981], and (4) as discussed above, the constant volcanic migration rate of 2.30 cm/yr to 2.38 cm/yr in a direction of S55°W is consistent with a deep-sourced plume fixed with respect to North American plate motion. The very high track rates prior to 10 Ma are somewhat mitigated if the track of the hotspot tail does not include the McDermitt and Owyhee-Humboldt volcanic fields (Figure 6e), as, for example, was suggested by *Geist and Richards* [1993].

6. Conclusion

We used data made available by a deep drill hole (WO-2) in the eastern Snake River Plain to correlate units north and south of the Plain and to assess new locations for the first major eruption in two of the largest volcanic fields associated with the track of the Yellowstone hotspot—the Heise and Picabo volcanic fields. We used new locations to calculate the migration rate of silicic volcanism between 10.27 Ma and 2.13 Ma of 2.30 cm/yr and between 6.66 Ma and 2.13 Ma of 2.35 cm/yr. These rates compare closely to the migration rate of our newly determined Yellowstone hotspot deformation field velocity of 2.38 ± 0.21 cm/yr which falls within the previous estimates of North American plate velocity of 2.2 cm/yr, 2.4 cm/yr, and 2.68 cm/yr based on previous global hotspot reference frame studies. From this we conclude that the migration rate of the Yellowstone-Snake River Plain silicic volcanic system is consistent in both direction and rate with a fixed mantle source being overridden by the North American plate during the last 10 m.y. These data combined with recent seismic tomography imaging, and helium isotopic studies support the classical deep-sourced hotspot model for Yellowstone.

Acknowledgments

We appreciate the help William C. Hackett provided in the early stages of this study and for providing us a description of the WO-2 core. Also, we thank Linda Davis of the USGS/INEEL for helping M.H.A. and G.F.E. with examination of the WO-2 core and helpful discussions with Dick Smith, Mike McCurry, and Mathias Obrebski. The text was greatly helped by reviews by Shan de Silva, Eric Christiansen, Mark Behn, Derek Schutt, Tom Parsons, and an anonymous reviewer. We thank Maureen M. Anders for helping with the figures and Claude Froidevaux, Dave Adams, Bill Phillips, and Dave Love for sampling various units used in this study and Joel Gombiner for helping with the $^{40}Ar/^{39}Ar$ analysis.

References

Allmendinger, R. W. (1982), Sequence of late Cenozoic deformation in the Blackfoot Mountains, southeastern Idaho, in *Cenozoic Geology of Idaho*, Idaho Bur. Min. Geol. Bull., vol. 26, edited by B. Bonnichsen and R. M. Breckenridge, pp. 505–516.

Anders, M. H. (1990), Late Cenozoic evolution of Grand and Swan Valley, Idaho, in *Geologic Field Tours of Western Wyoming and Parts of Adjacent Idaho*, in *Geological Survey of Wyoming Public Information Circular*, vol. 29, edited by S. Roberts, pp. 14–25, Laramie, Wyo.

Anders, M. H. (1994), Constraints on North American plate velocity from the Yellowstone hotspot deformation field, *Nature*, *369*, 53–55.

Anders, M. H., and N. H. Sleep (1992), Magmatism and extension: The thermal and mechanical effects of the Yellowstone hotspot, *J. Geophys. Res.*, *97*(B11), 15,379–15,393.

Anders, M. H., J. W. Geissman, L. A. Piety, and J. T. Sullivan (1989), Parabolic distribution of circum eastern Snake River Plain seismicity and latest Quaternary faulting: Migratory pattern and association with the Yellowstone hotspot, *J. Geophys. Res.*, *94*(B2), 1589–1621.

Anders, M. H., M. Spiegelman, D. W. Rodgers, and J. T. Hagstrum (1993), The growth of fault-bounded tilt blocks, *Tectonics*, *12*(6), 1451–1459.

Anders, M. H., J. Saltzman, and W. R. Hackett (1997), Borehole WO-2, The Rosetta stone [core] of the Heise Volcanics of east-central Idaho, Implications for the track of the Yellowstone hotspot, *Geol. Soc. Am. Abstr. Progr.*, *29*(6), A-365.
Anders, M. H., J. Saltzman, and S. R. Hemming (2009), Neogene tephra correlations in eastern Idaho and Wyoming: Implications for Yellowstone hotspot-related volcanism and tetonic activity, *Geol. Soc. Am. Bull.*, *121*, 837–856.
Arason, P., and S. Levi (2010), Maximum likelihood solution for inclination-only data in paleomagnetism, *Geophys. J. Int.*, *182*, 753–771.
Armstrong, R. L., W. P. Leeman, and H. F. Malde (1975), K-Ar dating, Quaternary and Neogene volcanic rocks of the Snake River Plain, Idaho, *Am. J. Sci.*, *275*, 225–251.
Bindeman, I. N., K. E. Watts, A. K. Schmitt, L. A. Morgan, and P. W. C. Shanks (2007), Voluminous low $\delta^{18}O$ magmas in the late Miocene Heise volcanic field, Idaho: Implications for the fate of Yellowstone hotspot calderas, *Geology*, *35*(11), 1019–1022.
Bonnichsen, B., W. P. Leeman, N. Honjo, W. C. McIntosh, and M. M. Godchaux (2008), Miocene silicic volcanism in southwestern Idaho: Geochronology, geochemistry and evolution of the central Snake River Plain, *Bull. Volcanol.*, *70*, 315–342.
Boroughs, S., J. Wolff, B. Bonnichsen, M. Godchaux, and P. Larson (2005), Large volume, low-$\delta^{18}O$ rhyolites of the central Snake River Plain, Idaho, USA, *Geology*, *33*, 821–824.
Branney, M. J., B. Bonnichsen, G. D. M. Andrews, B. Ellis, T. L. Barry, and M. McCurry (2008), "Snake River [SR]-type" volcanism at the Yellowstone hotspot track: Distinctive products from unusual, high-temperature silicic super-eruptions, *Bull. Volcanol.*, *70*, 293–314.
Brott, C. A., D. D. Blackwell, and J. P. Ziagos (1981), Thermal and tectonic implications of heat flow in the eastern Snake River Plain, Idaho, *J. Geophys. Res.*, *86*, 11,709–11,734.
Byrd, J. O. D., R. B. Smith, and J. W. Geissman (1994), The Teton fault, Wyoming: Topographic signature, neotectonics, and mechanism of deformation, *J. Geophys. Res.*, *99*(B10), 20,095–20,122.
Camp, V. E., and M. E. Ross (2004), Mantle dynamics and genesis of mafic magmatism in the intermountain Pacific Northwest, *J. Geophys. Res.*, *109*, B08204, doi:10.1029/2003JB002838.
Carr, W. J., and D. E. Trimble (1963), Geology of the American Falls Quadrangle, Idaho, *U. S. Geol. Surv. Bull.*, *1121-G*, 44.
Chadwick, J. D., D. W. Rodgers, and S. P. Payne (2007), Contemporary tectonic motion of the eastern Snake River Plain, Idaho: A global positioning system study, 1995–2004, *Tectonics*, *26*, TC6005, doi:10.1029/2005TC001914.
Channell, J. E. T., D. A. Hodell, B. S. Singer, and C. Xuan (2010), Reconciling astrochronological and $^{40}Ar/^{39}Ar$ ages for the Matuyama–Brunhes boundary and late Matuyama Chron, *Geochem. Geophys. Geosyst.*, *11*, Q0AA12, doi:10.1029/2010GC003203.
Christiansen, R. L. (2001), The Quaternary and Pliocene Yellowstone plateau volcanics field of Wyoming, Idaho, and Montana, U.S. Geol. Surv. Prof. Paper 729-G, pp. 145.
Christiansen, R. L., and J. D. Love (1978), The Pliocene Conant Creek Tuff in the northern part of the Teton Range and Jackson Hole, Wyoming, *U. S. Geol. Surv. Bull.*, *1435-C*, 9.
Christiansen, R. L., G. R. Foulger, and J. R. Evans (2002), Upper-mantle origin of the Yellowstone hotspot, *Geol. Soc. Am. Bull.*, *114*(10), 1245–1256.
Class, C., and S. L. Goldstein (2005), Evolution of helium isotopes in the Earth' s mantle, *Nature*, *436*(7054), 1107–1112.
Dalrymple, G. B. (1979), Critical tables for conversion of K-Ar ages from old to new constants, *Geology*, *7*, 558–560.
DeNosaquo, K. R., R. B. Smith, and A. R. Lowry (2009), Density and lithospheric strength models of the Yellowstone–Snake River Plain volcanic system from gravity and heat flow data, *J. Volcanol. Geotherm. Res.*, *188*, 108–127.
Doherty, D. J., L. A. McBroome, and M. A. Kuntz (1979), Preliminary geologic interpretation and lithologic log of the exploratory test well (INEL-1), Idaho National Engineering Laboratory, eastern Snake River Plain, Idaho, *U.S. Geol. Surv. Open File Rep.*, *79-124B*.
Drew, D. L., I. N. Bindeman, K. E. Watts, A. K. Schmitt, B. Fu, and M. McCurry (2013), Crustal-scale recycling in caldera complexes and rift zones along the Yellowstone hotspot track: O and Hf isotopic evidence in diverse zircons from voluminous rhyolites of the Picabo volcanic field, Idaho, *Earth Planet. Sci. Lett.*, *381*, 63–77.
Ellis, B. S., D. F. Mark, C. J. Pritchard, and J. A. Wolff (2012), Temporal dissection of the Huckleberry Ridge Tuff using the 40Ar/39Ar dating technique, *Quat. Geochronol.*, *9*, 34–41.
Embree, G. F., L. A. McBroome, and D. J. Doherty (1982), Preliminary stratigraphic framework of the Pliocene and Miocene rh rhyolite, eastern Snake River Plain, Idaho, in *Cenozoic Geology of Idaho*, Idaho Bur. Min. Geol. Bull., vol. 26, edited by B. Bonnichsen and R. M. Breckenridge, pp. 333–343.
Faccenna, C., T. W. Becker, S. Lallemand, Y. Lagabrielle, F. Funiciello, and C. Piromallo (2010), Subduction-triggered magmatic pulses: A new class of plumes?, *Earth Planet. Sci. Lett.*, *299*, 54–68.
Fisher, R. A. (1953), Dispersion on a sphere, *Proc. R. Soc. London, Ser. A*, *217*, 295–305.
Fouch, M. J. (2012), The Yellowstone hotspot: Plume or not?, *Geology*, *40*, 479–480.
Garwood, D. L., J. D. Kauffman, and K. L. Othberg (2011), Geologic map of the Picabo Quadrangle, in *Idaho Geologic Survey*, scale 1:24,000, University of Idaho, Missoula, Idaho.
Geist, D., and M. Richards (1993), Origin of the Columbia Plateau and Snake River plain: Deflection of the Yellowstone plume, *Geology*, *21*, 789–792.
Gilbert, J. D., D. A. Ostenaa, and C. K. Wood (1983), Seismotectonic study for Jackson Lake Dam and Reservoir, Minidoka Project, Idaho-Wyoming, Boise, Idaho, and Denver, Colorado, U.S. Bur. Rec., Pacific Northwest Regional Office and Engineering and Research Center, Seismotectonic Report 83-8, pp. 123.
Graham, D. W., M. R. Reid, B. T. Jordan, A. L. Grunder, W. P. Leeman, and J. E. Lupton (2009), Mantle source provinces beneath the north-western USA delimited by helium isotopes in young basalts, *J. Volcanol. Geotherm. Res.*, *188*(1–3), 128–140.
Gripp, A. E., and R. G. Gordon (1990), Current plate velocities relative to the hotspots incorporating the NUVEL-1 Global plate motion model, *Geophys. Res. Lett.*, *17*(8), 1109–1112.
Gripp, A. E., and R. G. Gordon (2002), Young tracks of hotspots and current plate velocities, *Geophys. J. Int.*, *150*(2), 321–361.
Hackett, W. R., and L. A. Morgan (1988), Explosive basaltic and rhyolitic volcanism of the eastern Snake River Plain, Idaho, in *Guidebook to the Geology of Central Idaho*, Idaho Geol. Surv. Bull., vol. 27, edited by P. K. Link and W. R. Hackett, pp. 283–301.
Henry, C. D., and J. A. Wolff (1992), Distinguishing strongly rheomorphic tuffs from extensive silicic lavas, *Bull. Volcanol.*, *54*, 171–186.
Henshaw, N. D. (2002), Temperature of silicic magmas from the Yellowstone hotspot, University of Utah, MS thesis, 362 pp., Salt Lake City, Utah.
Hildreth, E. W. (1977), The magma chamber of the Bishop Tuff: Gradients in temperature, pressure, and composition, PhD dissertation, pp. 328, University of California, Berkeley, Calif.
Hladky, F. R., K. S. Kellogg, S. S. Oriel, P. K. Link, J. W. Nielson, and R. E. Amerman (1992), Geologic map of the eastern part of the Fort Hall Indian Reservation, Bannock, Bingham, and Caribou counties, Idaho, U.S. Geol. Surv. IMAP 2006, scale 1:50,000.
Holmes, A. A. J., D. W. Rodgers, and S. S. Hughes (2008), Kinematic analysis of fractures in the Great Rift, Idaho: Implications for subsurface dike geometry crustal extension and magma dynamics, *J. Geophys. Res.*, *113*, B04202, doi:10.1029/2006JB004782.

Honjo, N., K. R. McElwee, R. A. Duncan, and W. P. Leeman (1986), K-Ar ages of volcanic rocks from the Magic Reservoir eruptive center, Snake River Plain, Idaho, *Isochron West*, *46*, 15–19.
Hough, B. G. (2001), Temporal constraints on crustal flexure adjacent to the eastern Snake River Plain, Idaho, Idaho State University, MS thesis, 75 pp., Pocatello, Idaho.
Humphreys, E. D., K. G. Dueker, D. L. Schutt, and R. B. Smith (2000), Beneath Yellowstone: Evaluating plume and nonplume models using teleseismic images of the upper mantle, *GSA Today*, *10*, 1–7.
James, D. E., M. J. Fouch, R. W. Carlson, and J. B. Roth (2011), Slab fragmentation, edge flow and the origin of the Yellowstone hotspot track, *Earth Planet. Sci. Lett.*, *311*, 124–135.
Jordan, B. T., A. L. Grunder, R. A. Duncan, and A. L. Deino (2004), Geochronology of age-progressive volcanism of the Oregon High Lava Plains: Implications for the plume interpretation of Yellowstone, *J. Geophys. Res.*, *109*, B10202, doi:10.1029/2003JB002776.
Kelbert, A., G. D. Egbert, and C. de Groot-Hedlin (2012), Crust and upper mantle electrical conductivity beneath the Yellowstone Hotspot Track, *Geology*, *40*, 447–450.
Kellogg, K. S., and G. F. Embree (1986), Geologic map of the Stevens Peak and Buckskin basin areas, Bingham and Bannock Counties, Idaho, U.S. Geol. Surv. Misc. Field Study Map MF-1854, scale 1:24,000.
Kellogg, K. S., S. S. Harlan, H. H. Mehnert, L. W. Snee, K. L. Pierce, W. R. Hackett, and D. W. Rodgers (1994), Major 10.2 Ma rhyolitic volcanism in the eastern Snake River Plain, Idaho—Isotopic age and stratigraphic setting of the Arbon Valley Tuff member of the Starlight Formation, *U.S. Geol. Surv. Bull., 2091*, pp. 18.
Kirkham, V. R. D. (1927), A geologic reconnaissance of Clark and Jefferson and parts of Butte, Custer, Fremont, Lemhi, and Madison counties, Idaho, *Idaho Bur. Min. Geol.*, *19*, 1–47.
Kirkham, V. R. D. (1931), The Snake River downwarp, *J. Geol.*, *39*, 456–482.
Kuiper, K. F., A. Deino, F. J. Hilgen, W. Krijgsman, P. R. Renne, and J. R. Wijbrans (2008), Synchronizing rock clocks of Earth history, *Science*, *320*, 500–504.
Kuntz, M. A., et al. (2003), Geologic map of the northern and central parts of the Idaho National Engineering and Environmental Laboratory, Eastern Idaho, Idaho Geol. Surv., Geol. Map 35.
Leeman, W. P. (1982a), Development of the Snake River Plain-Yellowstone Plateau Province, Idaho and Wyoming: An overview and petrologic model, in *Cenozoic Geology of Idaho*, Idaho Bur. Min. Geol. Bull., vol. 26, edited by B. Bonnichsen and R. M. Breckenridge, pp. 155–178.
Leeman, W. P. (1982b), Geology of the Magic Reservoir Area, Snake River Plain, Idaho, in *Cenozoic Geology of Idaho*, Idaho Bur. Min. Geol. Bull., vol. 26, edited by B. Bonnichsen and R. M. Breckenridge, pp. 369–376.
Leeman, W. P., C. Annen, and J. Dufek (2008), Snake River Plain–Yellowstone silicic volcanism: Implications for magma genesis and magma fluxes, in *Dynamics of Crustal Magma Transfer, Storage and Differentiation*, Geol. Soc., vol. 304, pp. 235–259, Spec. Publ., London.
Lipman, P. W. (1997), Subsidence of ash-flow calderas: Relations to caldera size and magma chamber geometry, *Bull. Volcanol.*, *59*, 198–218.
Love, J. D., J. C. Reed Jr., and A. C. Christiansen (1992), Geologic map of Grand Teton National Park, Teton county, Wyoming, U.S. Geol. Surv. Misc. Invest. Map I -2031, scale 1:62,500.
Mabey, D. R., D. L. Peterson, and C. Wilson (1974), Preliminary gravity map of southern Idaho, U.S. Geol. Surv. Open-File Rep. 74-78, scale 1:500,000.
Manley, C. R., and J. H. Fink (1987), Internal textures of rhyolitic flows as revealed by drilling, *Geology*, *15*, 549–552.
Mansfield, G. R., and C. S. Ross (1935), Welded rhyolitic tuffs in southeastern Idaho: Washington, D.C., Trans. Am. Geophys. Union, 16th Annual Meeting, 308-321.
Marvin, R. F., H. H. Mehnert, and D. C. Noble (1970), Use of ^{36}Ar to evaluate the incorporation of air by ash flows, *Geol. Soc. Am. Bull.*, *81*, 3385–3392.
Mazurek, J. (2004), Genetic controls on basalt alteration within the eastern Snake River Plain aquifer system, Idaho, MS thesis, pp. 215, Idaho State University, Pocatello, Idaho.
McBroome, L. A. (1981), Stratigraphy and origin of Neogene ash-flow tuffs on the north-central margin of the eastern Snake River Plain, Idaho, MS thesis, 74 pp., University of Colorado, Boulder, Colo.
McBroome, L. A., D. J. Doherty, and G. F. Embree (1982), Correlation of major Pliocene and Miocene rhyolites, eastern Snake River Plain, Idaho, Geol. Soc. Montana Guidebook, Southwest Montana Field Conference, 323-330.
McCurry, M., and D. W. Rodgers (2009), Mass transfer along the Yellowstone hotspot track I: Petrologic constraints on the volume of mantle-derived magma, *J. Volcanol. Geotherm. Res.*, *188*, 86–98.
Michalek, M. (2009), Age and amount of crustal flexure in the Lake Hills, south-central Idaho, and implications for the subsidence of the Eastern Snake River Plain, MS thesis, pp. 111, Idaho State University, Pocatello, Idaho.
Min, K., R. Mundil, P. R. Renne, and K. R. Ludwig (2000), A test for systematic errors in 40Ar/39Ar geochronology through comparison with U/Pb analysis of a 1.1-Ga rhyolite, *Geochim. Cosmochim. Acta*, *64*, 73–98.
Minster, J. B., and T. H. Jordan (1978), Present-day plate motion, *J. Geophys. Res.*, *83*(B11), 5331–5354.
Montelli, R., G. Nolet, F. A. Dahlen, G. Masters, E. R. Engdahl, and S. H. Hung (2004), Finite-frequency tomography reveals a variety of plumes in the mantle, *Science*, *303*(5656), 338–343.
Morgan, W. J. (1971), Convection plumes in the lower mantle, *Nature*, *230*, 42–43.
Morgan, W. J. (1972), Plate motions and deep-mantle convection, *Geol. Soc. Am. Mem.*, *132*, 7–22.
Morgan, L. A. (1988), Explosive rhyolitic volcanism on the eastern Snake River Plain, PhD thesis, 191 pp., University of Hawaii, Manoa, Hawaii.
Morgan, L. A. (1992), Stratigraphic relations and paleomagnetic and geochemical correlations of ignimbrites of the Heise volcanic field, eastern Snake River Plain, Eastern Idaho and Western Wyoming, in *Regional Geology of Eastern Idaho Western Wyoming*, Geological Society of America Memoir, vol. 179, edited by P. K. Link, M. A. Kuntz, and L. B. Platt, pp. 215–26.
Morgan, L. A., and W. C. McIntosh (2005), Timing and development of the Heise volcanic field, Snake River Plain, Idaho, western USA, *Geol. Soc. Am. Bull.*, *117*, 288–306.
Morgan, L. A., D. J. Doherty, and W. P. Leeman (1984), Ignimbrites of the eastern Snake River Plain: Evidence for major caldera-forming eruptions, *J. Geophys. Res.*, *89*, 8665–8678.
Obrebski, M., R. M. Allen, M. Xue, and S.-H. Hung (2010), Slab-plume interaction beneath the Pacific Northwest, *Geophys. Res. Lett.*, *37*, L14305, doi:10.1029/2010GL043489.
Obrebski, M., R. M. Allen, F. Pollitz, and S.-H. Hung (2011), Lithosphere-asthenosphere interaction beneath the western United State from the joint inversion of body-wave travel times and surface-wave phase velocities, *Geophys. J. Int.*, *185*, 1003–1021.
Pankratz, L. W., and H. D. Ackermann (1982), Structure along the northwest edge of the Snake River Plain interpreted from seismic refraction, *J. Geophys. Res.*, *87*(B4), 2676–2682.
Parsons, T., and G. A. Thompson (1991), The role of magma overpressure in suppressing earthquakes and topography: Worldwide examples, *Science*, *253*(5026), 1399–1402.

Parsons, T., G. A. Thompson, and R. P. Smith (1998), More than one way to stretch: A tectonic model for extension along the plume track of the Yellowstone hotspot and adjacent Basin and Range Province, *Tectonics*, *17*, 221–234.
Payne, S. J., R. McCaffrey, and R. W. King (2008), Strain rates and contemporary deformation in the Snake River Plain and surrounding Basin and Range from GPS and seismicity, *Geology*, *36*, 647–650.
Payne, S. J., R. McCaffrey, R. W. King, and S. A. Kattenhorn (2012), A new interpretation of deformation rates in the Snake River Plain and adjacent basin and range regions based on GPS measurements, *Geophys. J. Int.*, *189*, 101–122.
Perkins, M. E., and B. P. Nash (2002), Explosive silicic volcanism of the Yellowstone hotspot: The ash fall tuff record, *Geol. Soc. Am. Bull.*, *114*(3), 367–381.
Pierce, K. L., and L. A. Morgan (1992), The track of the Yellowstone hotspot: Volcanism, faulting, and uplift, in *Regional Geology of Eastern Idaho and Western Wyoming*, Geol. Soc. Am. Mem., vol. 179, edited by P. K. Link, M. A. Kuntz, and L. B. Platt, pp. 1–53.
Pierce, K. L., and L. A. Morgan (2009), Is the track of the Yellowstone hotspot driven by a deep mantle plume?—Review of volcanism, faulting, and uplift in light of new data, *J. Volcanol. Geotherm. Res.*, *188*, 1–25.
Pierce, K. L., L. A. Morgan, and R. W. Saltus (2002), Yellowstone plume head: Postulated tectonic relations to the Vancouver slab, continental boundaries, and climate, in *Tectonic and Magmatic Evolution of the Snake River Plain Volcanic Province*, Idaho Geol. Surv. Bull., vol. 30, edited by B. Bonnichsen, C. M. White, and M. McCurry, pp. 5–33.
Piety, L. A., C. K. Wood, J. D. Gilbert, J. T. Sullivan, and M. H. Anders (1986), Seismotectonic study for Palisades Dam and Reservoir, Palisades Project, U.S. Bur. Rec., Seismotectonics Rep. 86-3.
Price, K. B. (2009), Geology of the northern end of the Big Hole Mountains, Madison County, Idaho, Idaho State University, MS thesis, 120 pp., Pocatello, Idaho.
Prostka, H. J., and G. F. Embree (1978), Geology and geothermal resources of the Rexburg area, eastern Idaho, *U.S. Geol. Surv. Open File Rep.*, *78-1009*, pp. 14, 2 pls.
Prostka, H. J., G. F. Embree, and D. J. Doherty (1979), The Pliocene Rexburg caldera complex, southeastern Idaho, *Geol. Soc. Am. Abstr. Progr.*, *11*, 499.
Renne, P. R., C. C. Swisher, A. L. Deino, D. B. Karner, T. Owens, and D. J. DePaolo (1998), Intercalibration of standards, absolute ages and uncertainties in $^{40}Ar/^{39}Ar$ dating, *Chem. Geol. (Isotope Geosci. Sect.)*, *145*(1-2), 117–152.
Renne, P. R., R. Mundil, G. Balco, K. W. Min, and K. R. Ludwig (2010), Joint determination of K-40 decay constants and Ar-40*/K-40 for the Fish Canyon sanidine standard, and improved accuracy for Ar-40/Ar-39 geochronology, *Geochim. Cosmochim. Acta*, *74*(18), 5349–5367.
Renne, P. R., G. Balco, K. Ludwig, R. Mundil, and K. Min (2011), Response to the comment by W. H. Schwarz et al. on "Joint determination of ^{40}K decay constants and $^{40}Ar^*/^{40}K$ for the Fish Canyon sanidine standard, and improved accuracy for $^{40}Ar/^{39}Ar$ geochronology" by P. R. Renne et al. (2010), *Geochim. Cosmochim. Acta*, *75*, 5097–5100.
Reynolds, R. L. (1975), Paleomagnetism of the Yellowstone tuffs and their associated air-fall ashes, PhD thesis, 268 pp., University of Colorado, Boulder, Colo.
Ribe, N. M., and U. R. Christensen (1994), Three-dimensional modeling of plume-lithosphere interaction, *J. Geophys. Res.*, *99*, 669–682.
Rodgers, D. W., and M. H. Anders (1990), Neogene evolution of Birch Creek Valley near Lone Pine, Idaho, in *Geologic Field Tours of Western Wyoming and Parts of Adjacent Idaho, Montana and Utah*, Geol. Surv., vol. 29, edited by S. Roberts, pp. 26–38, Pub. Info. Circ, Laramie, Wyo.
Rodgers, D. W., W. R. Hackett, and H. T. Ore (1990), Extension of the Yellowstone plateau, eastern Snake River Plain, and Owyhee plateau, *Geology*, *18*(11), 1138–1141.
Rodgers, D. W., H. T. Ore, R. T. Bobo, N. McQuarrie, and N. Zentner (2002), Extension and subsidence of the eastern Snake River Plain, Idaho, in *Tectonic and Magmatic Evolutions of the Snake River Plain Volcanic Province*, Idaho Geol. Surv. Bull., vol. 30, edited by B. Bonnichsen, C. W. White and M. McCurry, pp. 121–155.
Rodgers, D. W., S. P. Long, N. McQuarrie, W. D. Burgel, and C. Hensely (2006), Geologic map of the Inkom 7.5′ Quadrangle, Bannock County, Idaho, Idaho Geol. Surv. Tech. Report 06-2, scale 1:24,000.
Rosenbaum, J. G. (1986), Paleomagnetic direction dispersion produced by plastic deformation in a thick Miocene welded tuff, southern Nevada, *J. Geophys. Res.*, *91*, 12,817–12,834.
Saltzer, R., and E. Humphreys (1997), Upper mantle *P* wave structure of the eastern Snake River Plain and its relationship to geodynamic models of the region, *J. Geophys. Res.*, *102*(B6), 11,829–11,841.
Schmandt, B., K. Dueker, E. Humphreys, and S. Hansen (2012), Hot mantle upwelling across the 660 beneath Yellowstone, *Earth Planet. Sci. Lett.*, *331*, 224–236.
Schmidt, D. L. (1961), Quaternary geology of the Bellevue area in Blaine and Camas counties, Idaho, PhD dissertation, 127 pp., University of Washington, Seattle, Wash.
Schmidt, D. L. (1962), Quaternary geology of the Bellevue area in Blaine and Camas counties, Idaho, *U.S. Geol. Surv. Open File Rep.*, *62-0120*, pp. 107.
Shervais, J. W., and B. B. Hanan (2008), Lithospheric topography, tilted plumes, and the track of the Snake River-Yellowstone Hotspot, *Tectonics*, *27*, TC5004, doi:10.1029/2007TC002181.
Simpson, D. W., and M. H. Anders (1992), Tectonics and topography of the western U.S.: An example of digital map making, *GSA Today*, *2*, 118–121.
Skipp, B. (1984), Geologic map and cross sections of the Italian Peak and Italian Peak Middle Roadless Areas, Beaverhead County, Montana, and Clark and Lemhi Counties, Idaho, U.S. Geol. Surv. Misc. Field Stud. Map MF-1601-B, map scale 1:62,500.
Smith, R. B., and L. W. Braile (1994), The Yellowstone hotspot, *J. Volcanol. Geotherm. Res.*, *61*, 121–187.
Smith, R. B., J. Jordan, B. Steinberger, C. M. Puskas, J. Farrell, G. P. Waite, S. Husen, W.-L. Chang, and R. O. O'Connell (2009), Geodynamics of the Yellowstone hotspot and mantle plume: Seismic and GPS imaging, kinematics, and mantle flow, *J. Volcanol. Geotherm. Res.*, *188*, 26–56.
Snider, L. G. (1995), Stratigraphic framework, geochemistry, geochronology, and eruptive styles of Eocene volcanic rocks in the White Knob Mountains area, southeastern Challis volcanic field, central Idaho: Idaho State University, MS thesis, 212 pp., Pocatello, Idaho.
Stearns, H. T., and I. Isotoff (1956), Stratigraphic sequence in the Eagle Rock volcanic area near American Falls, Idaho, *Geol. Soc. Am. Bull.*, *67*, 19–34.
Suppe, J., C. Powell, and R. Berry (1975), Regional topography, seismicity, Quaternary volcanism, and the present-day tectonics of the Western United States, *Am. J. Sci.*, *275-A*, 397–436.
Taylor, J. R. (1982), *An Introduction to Error Analysis: The Study of Uncertainties in Physical Measurements*, pp. 327, Oxford Univ. Press, Sausalito, Calif.
Trimble, D. E. (1976), Geology of Micharud and Pocatello quadrangles, Bannock and Power County, Idaho, *US Geol. Surv. Bull.*, *1399*, 115 pp.
Wagner, L., D. W. Forsyth, M. J. Fouch, and D. E. James (2010), Detailed three-dimensional shear wave velocity structure of the northwestern United States from Rayleigh wave tomography, *Earth Planet. Sci. Lett.*, *299*(3), 273–284.

Watts, K. E., W. P. Leeman, I. N. Bindeman, and B. P. Larson (2010), Supereruptions of the Snake River Plain: Two-stage derivation of low-$\delta^{18}O$ rhyolites from normal-$\delta^{18}O$ crust as constrained by Archean xenoliths, *Geology*, *38*, 503–506.

Watts, K. E., I. N. Bindeman, and A. K. Schmitt (2011), Large-volume rhyolite genesis in caldera complexes of the Snake River Plain: Insights from the Kilgore Tuff of the Heise volcanic field, Idaho, with comparison to Yellowstone and Bruneau-Jarbidge rhyolites, *J. Petrol.*, *52*, 857–890.

Williams, P. L., H. R. Covington, and K. L. Pierce (1982), Cenozoic stratigraphy and tectonic evolution of the Raft River basin, in *Cenozoic Geology of Idaho*, Idaho Bur. Min. Geol. Bull., vol. 26, edited by B. Bonnichsen and R. M. Breckenridge, pp. 491–504.

Yuan, H., and K. Dueker (2005), Teleseismic P-wave tomogram of the Yellowstone plume, *Geophys. Res. Lett.*, *32*, L07304, doi:10.1029/2004GL022056.

Yuan, H., K. Dueker, and J. Stachnik (2010), Crustal structure and thickness along the Yellowstone hotspot track: Evidence for lower crustal outflow from beneath the eastern Snake River Plain, *Geochem. Geophys. Geosys.*, *11*, Q03009, doi:10.1029/2009GC002787.